Magma degassing in the effusive-explosive subglacial rhyolitic eruption of Dalakvísl, Torfajökull, Iceland: insights into quenching pressures, palaeo-ice thickness, and edifice erosion

Jacqueline Owen[a]*, Hugh Tuffen[a], Dave McGarvie[a]

[a]Lancaster Environment Centre, Lancaster University, Lancaster, LA1 4YQ. UK

*j.owen2@lancaster.ac.uk

1 Abstract

Dissolved volatile contents preserved in the matrix glass of subglacially erupted rocks offer important insights into quenching pressures. With careful interpretation, these data may yield information on eruption conditions. In this paper we present detailed edifice and glacier reconstructions for explosive and effusive subglacial rhyolitic deposits at Dalakvísl, Torfajökull, Iceland. When grouped by lithofacies, Dalakvísl glasses display trends of decreasing H_2O with elevation, consistent with a subglacial setting. A number of solubility pressure curves (SPCs) have been used to model these quenching pressure-elevation trends in order to reconstruct the loading conditions. Effusively erupted glasses (e.g. lava lobes) have higher dissolved water contents than the more explosively produced material (e.g. obsidian sheets), indicating a systematic difference in subglacial pressure and/or degassing behaviour. Best model fits to data are achieved when loading is by a combination of erupted deposits (with a flat-topped morphology) and ice/meltwater. Our best estimate for the original edifice summit elevation is ~810 m a.s.l., similar to its current elevation; however, as the edifice is now more conical this indicates significant post-eruptive erosion around the margins of the edifice. We propose that during the initial stages of the eruption, meltwater could not escape, thus maintaining high subglacial pressure under which effusive lava bodies were produced intrusively. Our best estimate is that the original palaeo-ice surface was ~1,020 m a.s.l., suggesting a syn-eruptive glacier thickness of ~350 m, assuming a similar base level to today (~670 m a.s.l.). A sudden release of meltwater then led to a pressure drop, driving a transition to more explosive activity with an ice surface over the vent closer to 880 m a.s.l. This study demonstrates the uses of dissolved volatile contents in reconstructing past environments and shows how eruption dynamics can be tracked over the timeline of a pre-historic eruption, offering valuable insight into the complex coupling between pressure and the mechanisms of subglacial eruptions.

Keywords subglacial · rhyolite · explosive-effusive transition · water solubility · infra-red spectroscopy · Iceland · volcano-ice interactions

2 Introduction

2.1 Research Goals

Although eyewitness accounts and monitoring of recent eruptions are perhaps the greatest source of accurate data, capturing such accounts can be difficult to achieve, especially for subglacial settings. Firstly, subglacial volcanoes can be extremely explosive due to violent fuel-coolant interactions and are therefore dangerous to monitor (Duncan et al., 1986; Mastin et al., 2004; Stevenson et al., 2011). Secondly, some, if not all, of the deposits will be obscured by the glacier (Tómasson, 1996; Owen, 2016). Thirdly, a subglacial rhyolite eruption has never been observed (Guðmundsson, 2003; Tuffen et al., 2008). Therefore, in order to understand subglacial rhyolitic volcanism, we need to turn to past eruptions (Owen, 2016).

This paper focuses on the subglacial rhyolite eruption at Dalakvísl in southern Iceland, which was part of one of Iceland's largest known subglacial rhyolitic eruptions, from Torfajökull at 70 ka (McGarvie et al., 2006; Tuffen et al., 2008). The Dalakvísl deposits record both explosive and effusive activity (Tuffen et al., 2008) and may provide insight into mechanisms of subglacial rhyolitic volcanism. Consequently it has been well studied: Tuffen et al. (2008) documented the erupted lithofacies; Owen et al. (2013a) measured pre-eruptive volatiles and reconstructed degassing paths for Dalakvísl and four other subglacial Torfajökull edifices, deducing that magmatic degassing was the main influence on eruptive style; and Owen et al. (2013b) incorporated dissolved volatile concentrations and vesicle textures to further investigate the transition in eruptive style at Dalakvísl, deducing that it coincided with and was likely caused by a sudden pressure drop, most likely triggered by a jökulhlaup.

This paper will use dissolved volatile concentrations from Owen et al. (2013b) to calculate quenching pressures in order to reconstruct the palaeo-ice thickness, eruptive setting (i.e. whether outcrops formed intrusively or extrusively), original edifice morphology and erosion history. This will aid future interpretations of subglacial rhyolitic lithofacies, improve understanding of the way in which subglacial rhyolitic edifices erode, shed light on past climates, and explore links between eruptive style and ice thickness.

2.2 Volatile-based palaeo-ice reconstructions

The majority of volcano based palaeo-ice reconstructions have relied on the elevation of subglacial-to-subaerial lithofacies transitions at tuyas; edifices where erupting material broke through the surface of ice sheets (Mathews, 1947; Jones, 1966; McGarvie et al., 2006;

Edwards et al., 2011; Owen, 2016). However, due to increased understanding of water solubility-pressure relationships (Newman et al., 1988; Dixon and Stolper, 1995; Dixon, 1997; Newman and Lowenstern, 2002) a new technique is being refined (Tuffen et al., 2010; Owen, 2016) whereby the dissolved water content of glassy eruptive material can be used to reconstruct quenching pressures (e.g. Saubin et al., 2016) and therefore estimate palaeo-ice thicknesses (Dixon et al., 2002; Höskuldsson et al., 2006; Schopka et al., 2006; Edwards et al., 2009; Owen et al., 2012).

The technique utilises the pressure dependence of water solubility in silicate melts. Rise and decompression of volatile-saturated magma results in volatile exsolution, which depletes the residual melt in dissolved volatiles (Gonnermann and Manga, 2007). Assuming equilibrium degassing, the dissolved volatile content in volcanic glasses should record the quenching pressure (Tuffen et al., 2010). In subglacial settings, this can be converted into palaeo-ice thicknesses so long as subglacial cavity pressure equals glaciostatic pressure from the overlying ice burden (Tuffen et al., 2010). However, non-glaciostatic pressure may develop, depending on the local volume flux (input of erupted material vs volume of ice melted) and extent of meltwater drainage (Guðmundsson et al., 2004; Tuffen et al., 2010). Furthermore, quenching pressure may reflect loading by rock, as well as ice or meltwater, giving a greater increase in pressure with elevation due to the higher density of the loading medium (Tuffen and Castro, 2009).

Although factors such as volatile undersaturated melt and non-glaciostatic pressure may hinder reconstructions of palaeo-ice thickness, such palaeo-pressure reconstructions may constrain aspects of subglacial hydrology (Höskuldsson et al., 2006; Schopka et al., 2006; Owen et al., 2013b), edifice erosion (Stevenson et al., 2009; Tuffen and Castro, 2009; Owen et al., 2012) and pre-eruptive volatile content (Dixon et al., 2002; McGarvie et al., 2007; Owen et al., 2012).

Another major advantage of this technique is that it is not limited to tuyas but is also applicable to non-emergent, wholly subglacial edifices.

2.3 Geological background

Iceland hosts >30 active volcanic systems, which typically consist of a central volcano and associated fissure swarms. Of these, at least 23 have produced subglacial rhyolite in the last 0.8 Ma (McGarvie, 2009). Rhyolitic volcanism is mostly limited to central volcanoes (Sigurdsson, 1977; Sæmundsson, 1979; Imsland, 1983), as rhyolite petrogenesis involves both fractional crystallisation and partial re-melting of the crust (Gunnarsson et al., 1998; Martin and Sigmarsson, 2007; Zellmer et al., 2008; Martin and Sigmarsson, 2010). As most Icelandic central volcanoes have erupted ~10% rhyolite (Imsland, 1983) and a third of 20th century Icelandic eruptions were subglacial (Guðmundsson, 2005) subglacial rhyolitic eruptions constitute an important part of past and future volcanism in Iceland.

Torfajökull central volcano is located in southern Iceland (**Fig. 1a**) where the Eastern Volcanic Zone (EVZ) propagates southwards into the Southern Flank Zone (SFZ). With 80% rhyolite (Gunnarsson et al., 1998) Torfajökull is Iceland's largest producer of silicic magma, attributed to enhanced melting of older crust (Sigurdsson, 1977; Martin and Sigmarsson, 2007). Torfajökull demonstrates a great diversity in subglacial rhyolitic edifices (Sæmundsson, 1972; McGarvie, 1984; McGarvie et al., 2006; McGarvie, 2009), ranging from small volume effusive edifices such as Bláhnúkur (**Fig. 1b**), consisting of lava lobes and quench hyaloclastite (Furnes et al., 1980; Tuffen et al., 2001; McGarvie, 2009), to steep-sided tuyas such as SE

Rauðfossafjöll (**Fig. 1b**), which consist of fine-grained pyroclastic material capped by subaerial lava flows (Tuffen et al., 2002; McGarvie, 2009).

The ~70 ka rhyolitic eruption from Torfajökull, with >16 km^3 total preserved erupted volume (McGarvie et al., 2006), is one of the largest known silicic eruptions in Iceland and the largest known subglacial rhyolite event. Edifices constructed during this eruption form a ring around Torfajökull (McGarvie et al., 2006), hereafter known as the ring fracture rhyolites (**Fig. 1b**). All ring fracture edifices may derive from a single eruptive event (MacDonald et al., 1990; McGarvie et al., 1990) for which two samples provide Ar-Ar dates of 67.2 ±9.1 ka and 71.5 ±7.4 ka (McGarvie et al., 2006). However, Brendryen et al. (2010) have also identified Torfajökull rhyolites in a North Atlantic marine core. Similar compositions and ages (Brendryen et al., 2010) suggest these layers represent ring fracture rhyolites. These North Atlantic ash layers indicate that an additional significant volume of ash was widely distributed out to sea during this event, requiring higher estimates of the total erupted volume. Furthermore, interspersing of the rhyolitic layers with basaltic horizons over an 800 year period (Brendryen et al., 2010), challenges the model for a single eruptive event (MacDonald et al., 1990; McGarvie et al., 1990), instead favouring a scenario where the ring fracture rhyolites erupted in pulses, over an 800 year period or more.

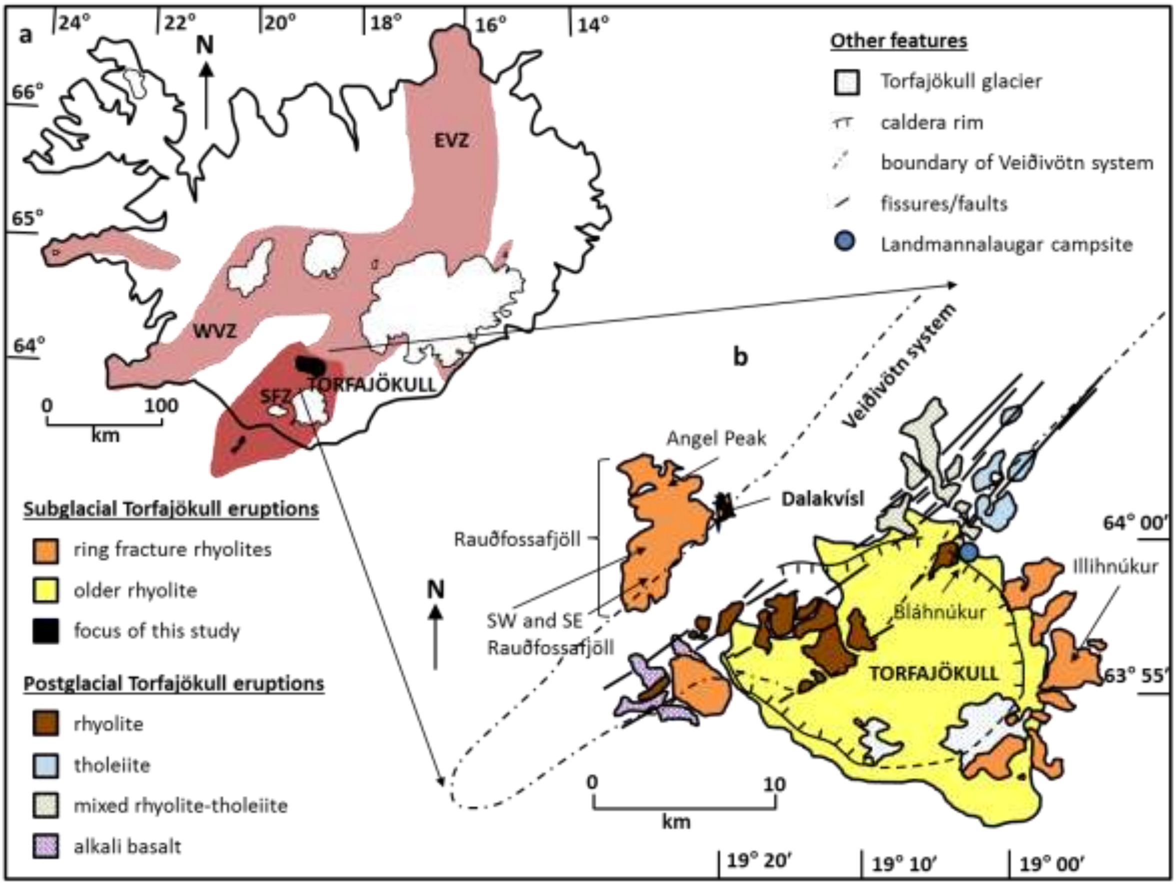

Figure 1: Maps modified from Owen et al. (2012): **(a)** Simplified geological map of Iceland, showing the location of Torfajökull, based on Larsen (1984) and Gunnarsson et al. (1998). WVZ: West Volcanic Zone, EVZ: East Volcanic Zone, SFZ: Southern Flank Zone. **(b)** Simplified geological map of Torfajökull, showing the location of Dalakvísl, based on Blake (1984), McGarvie (1984), Gunnarsson et al. (1998) and McGarvie et al. (2006).

Based on its geochemistry and position, Dalakvísl is one of the edifices attributed to the 70 ka event (Tuffen et al., 2008). It occurs at the northern fringe of the Rauðfossafjöll rhyolite massif in western Torfajökull (**Fig. 1b**), where there are four large tuyas, each exceeding 1 km^3 in volume and with 1,174-1,235 m summit elevations (Tuffen et al., 2002). By contrast, the summit elevation of Dalakvísl is 810 m and the deposit volume <0.2 km^3

(Tuffen et al., 2008). Nonetheless, fragmental lithofacies at Dalakvísl are similar to those at the Rauðfossafjöll tuyas, including fine-grained pumiceous pyroclastic deposits typical of explosive activity (Stevenson et al., 2011). Crudely bedded fragmental deposits at Dalakvísl (**Figs. 2di,ii**; 'cba' in **Figure 3**) suggest an aqueous subglacial setting and provide the first documented evidence for localised meltwater ponding during a subglacial rhyolitic eruption (Tuffen et al., 2008). However, Dalakvísl lithofacies also include lava lobe-bearing hyaloclastite (**Figs. 2ai,ii;** 'cj' in **Figure 3**) (Tuffen et al., 2008), which resembles the products of an effusive subglacial rhyolite eruption at Bláhnúkur, Torfajökull (Tuffen et al., 2001). The hyaloclastite consists of perlitised obsidian breccia and blocky, low vesicularity ash shards. Lava lobes are crudely conical, generally 5-10 m wide and 3-5 m thick, with a microcrystalline interior and dense obsidian carapace, and their vesicularity is generally < 5%. Columnar-jointed upper surfaces are thought to show ice contact, indicating that lava lobes formed within subglacial cavities at the glacier base (Tuffen et al., 2008).

The variety of explosive and effusive lithofacies at Dalakvísl therefore indicates that the eruption underwent a change in eruptive behaviour. A pyroclastic deposit containing obsidian sheets is of particular interest regarding the transition in eruptive style (**Figs. 2bi-iii**; 'os' in **Figure 3**). Sheets are 0.5-1 m thick and 1-20 m long lava bodies that occupy 10 volume % of a pumiceous pyroclastic breccia. They consist of three zones (**Fig. 2biii**): an inner core of relatively dense obsidian (zone 1) and an outer zone of pumice (zone 3), with a transitional zone separating the two (zone 2). The sheets have a jigsaw fit with the surrounding breccia, which is thought to be composed of earlier disintegrated sheets. As lava body size, vesicularity and grain size distribution for this deposit (Owen et al., 2013b) all fall between the lava lobe deposits (effusive endmember) and the crudely bedded ash (explosive endmember), the obsidian sheet deposit is thought to encapsulate transitional behaviour at Dalakvísl (Tuffen et al., 2008).

Tuffen et al. (2008) used obsidian sheet vesicle textures (**Fig. 2bii**) to propose formation when a vesiculating, incompletely fragmented magma intruded within overlying pyroclastic debris, triggering partial foam collapse that generated the sheets and drove a transition from explosive to effusive activity. This theory is contested by Stevenson et al. (2011) and Owen et al. (2013b), who favour a model of *in-situ* localised vesiculation.

Other lithofacies at Dalakvísl (**Fig. 3**) include perlitised lava, poorly exposed obsidian mounds (referred to as ‘miscellaneous’ or ‘misc.’ in figures) and remobilised deposits of obsidian sheets and lava lobes (referred to as ‘juxtaposed obsidian’ in figures) (**Figs. 2ci,ii**).

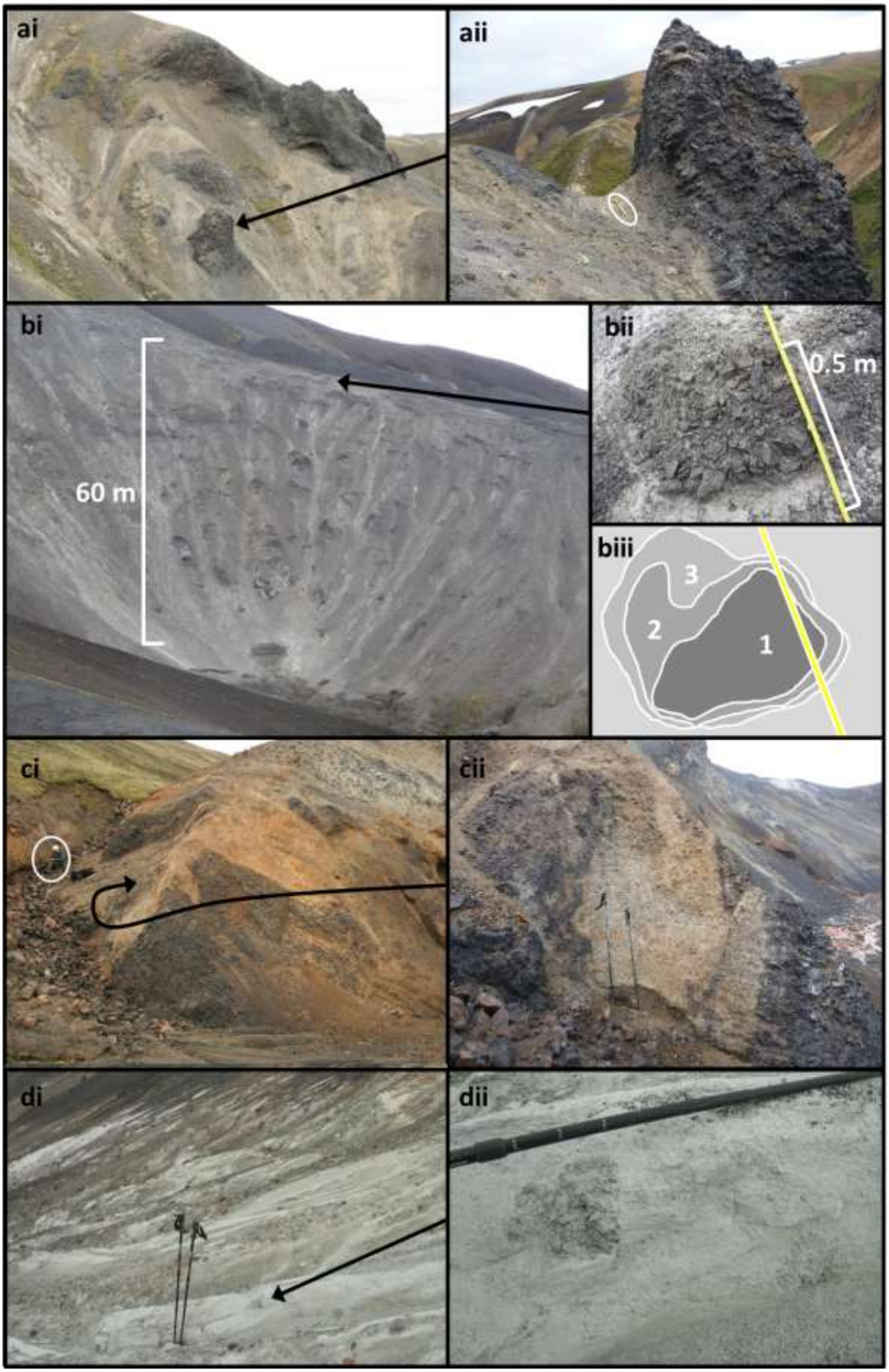

179

Figure 2: Dalakvísl lithofacies (see **Figure 3** for sample locations). **(ai)** Dark lava lobes (5-40 m long) protrude from massive obsidian and pumice breccia (looking NE towards D1-D4). **(aii)** A single columnar-jointed lava lobe (locality D1), with a geological hammer for scale (outlined with white circle). **(bi)** Dark obsidian sheets (1-10 m long) surrounded by pale ash-pumice breccia (looking N towards D11-D16). **(bii)** A small obsidian sheet with a metre rule for scale (locality D16). **(biii)** A schematic representation of **Figure 2bii**. Numbers indicate textural zones: 1 - dark grey vesicle-poor obsidian; 2- medium grey, moderately vesicular obsidian; 3 - pale grey pumice. **(ci)** A deposit of deformed sheet and lobe portions juxtaposed with variably vesicular obsidian and pumiceous breccia and cut through by faults (looking N towards D5) with person for scale (outlined with white circle). **(cii)** A more detailed view of the deposit in part **ci**, walking poles are 1.2 m long. **(di)** A deposit of crudely bedded ash (cba), looking W towards D7. **(dii)** A pumiceous clast within the cba deposit.

2.4 Previous constraints on the ice thickness at Dalakvísl

The syn-eruptive ice thickness at Dalakvísl, was estimated at 300-400 m (Tuffen et al., 2008) based on water concentrations in a single obsidian sheet. However, it is now clear that complex degassing patterns in even small-volume subglacial eruptions require multiple sampling for robust ice thickness measurements (Owen et al., 2012; Owen, 2016).

Thus, further work is needed to 1) better constrain the ice thickness at Dalakvísl 2) investigate different loading mediums to better understand where there has been intrusive and extrusive formation; and 3) understand subglacial pressure conditions in an eruption that straddled the explosive-effusive transition.

3 Methods

3.1 Sample collection

Twenty-nine obsidian samples were collected from 16 localities (**Fig. 3**) and are the same as those used in the Owen et al. (2013b) study. The samples encompass a wide range of elevations, lithofacies and positions (**Table 1**). All three textural zones within obsidian sheets were sampled (**Fig. 2biii**). All collected samples are glassy; those showing evidence for perlitisation or post-quenching movement were avoided. In addition, one ash sample (D7a) was collected for geochemical analysis.

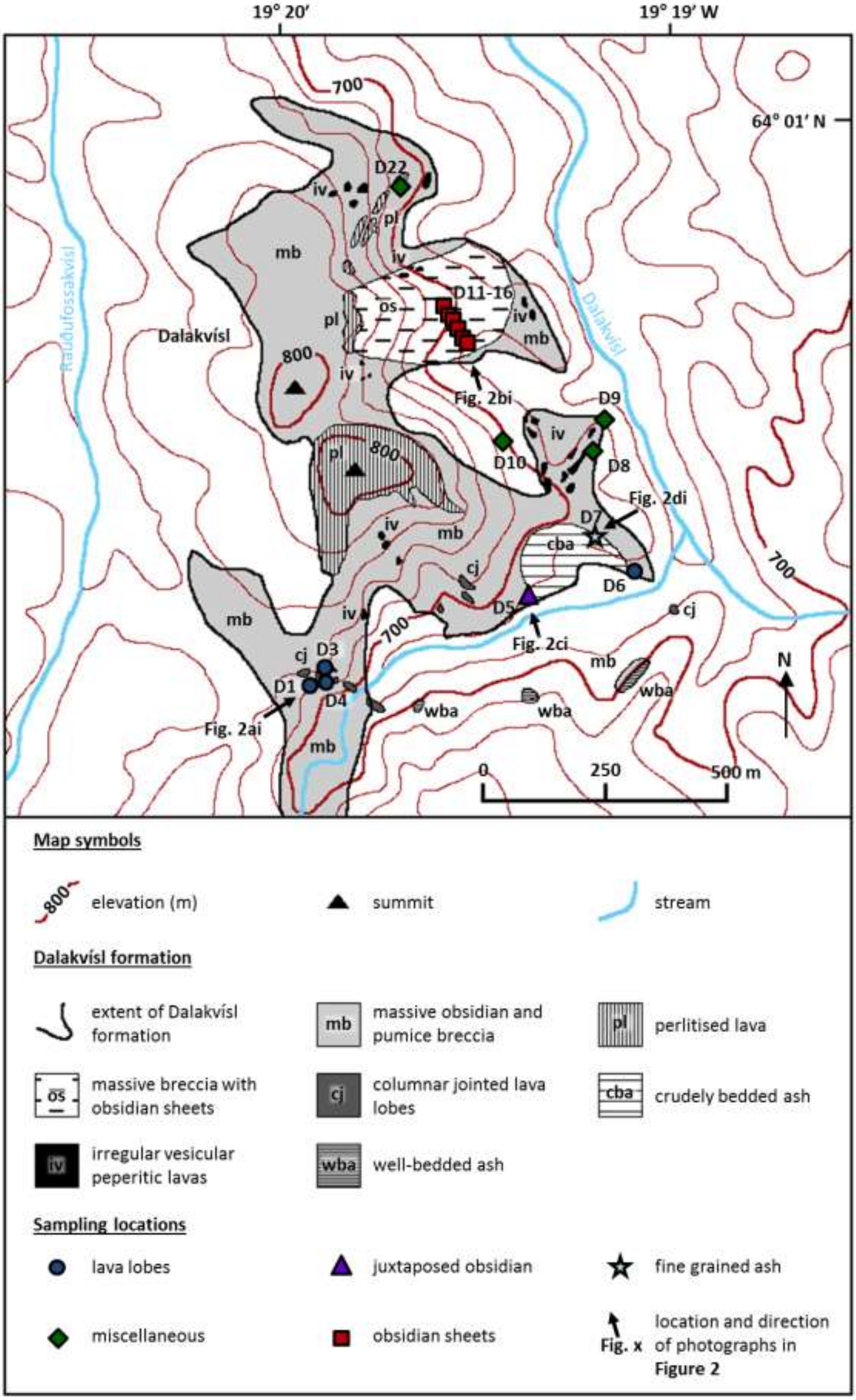
19° 20′
19° 19′ W
64° 01′ N
700
800
Dalakvísl
Rauðufossakvísl
Dalakvísl
D22
D11-16
D9
D10
D8
D7
D6
D5
D3
D1
D4
Fig. 2bi
Fig. 2di
Fig. 2ci
Fig. 2ai
mb
pl
iv
os
cba
cj
wba
N
0
250
500 m
Map symbols
elevation (m)
summit
stream
Dalakvísl formation
extent of Dalakvísl formation
massive obsidian and pumice breccia
perlitised lava
massive breccia with obsidian sheets
columnar jointed lava lobes
crudely bedded ash
irregular vesicular peperitic lavas
well-bedded ash
Sampling locations
lava lobes
juxtaposed obsidian
fine grained ash
miscellaneous
obsidian sheets
location and direction of photographs in Figure 2
Fig. x

Figure 3: A geological map of Dalakvísl, modified from Tuffen et al. (2008), showing the sampling locations. Coloured symbols represent lithofacies (**Table 1**) and are used throughout the paper as per the legend.

Table 1: A brief summary of sample descriptions, sampling locations and the analytical work done on each.

Sample name	GPS coordinates	Elevation (m) [a]	Reference facies unit [b]	Sample description [d]	Locality description	Inferred eruptive behaviour	FTIR	XRF	Figs. [g]
D1	N 64 00 22.6, W019 19 51.5	725	cj	ob	lava lobe	effusive	yes	yes	2ai,ii
D3	N 64 00 23.8, W019 19 53.2	760	cj	ob	lava lobe	effusive	yes	/	2ai,ii
D4		730	cj	ob	lava lobe	effusive	yes	/	2ai,ii
D5a	N 64 00 28.6, W019 19 18.3	680	iv/cj	ob	juxtaposed ob	? [f]	yes	/	2ci,ii
D5b	N 64 00 28.6, W019 19 18.3	680	iv/cj	pum	juxtaposed ob	? [f]	yes	/	2ci,ii
D6	N 64 00 30.0, W019 19 04.0	695	cj	ob	lava lobe	effusive	yes	/	/
D7a	N 64 00 32.2, W019 19 10.7	707	cba	ash	fine ash	explosive	/	yes	2di,ii
D7b	N 64 00 32.2, W019 19 10.7	707	cba	pum clast	fine ash	explosive	yes	/	2di,ii
D8	N 64 00 38.0, W019 19 10.7	701	iv	ob	misc. [e]	? [f]	yes	/	/
D9	N 64 00 40.0, W019 19 09.0	674	mb	ob	misc. [e]	? [f]	yes	/	/
D10	N 64 00 38.5, W019 19 24.6	725	pl [c]	ob	misc. [e]	? [f]	yes	/	/
D11a	N 64 00 45.0, W019 19 29.2	668	os	ob	sheet	transition	yes	/	2bi-iii
D11b	N 64 00 45.0, W019 19 29.2	668	os	tran	sheet	transition	yes	/	2bi-iii
D11c	N 64 00 45.0, W019 19 29.2	668	os	pum	sheet	transition	yes	/	2bi-iii
D12a	N 64 00 45.3, W019 19 29.8	678	os	ob	sheet	transition	yes	/	2bi-iii
D12b	N 64 00 45.3, W019 19 29.8	678	os	tran	sheet	transition	yes	/	2bi-iii
D12c	N 64 00 45.3, W019 19 29.8	678	os	pum	sheet	transition	yes	/	2bi-iii
D13a	N 64 00 45.3, W019 19 31.0	692	os	ob	sheet	transition	yes	yes	2bi-iii
D13b	N 64 00 45.3, W019 19 31.0	692	os	tran	sheet	transition	yes	/	2bi-iii
D13c	N 64 00 45.3, W019 19 31.0	692	os	pum	sheet	transition	yes	/	2bi-iii
D14a	N 64 00 46.3, W019 19 31.9	701	os	ob	sheet	transition	yes	/	2bi-iii
D14b	N 64 00 46.3, W019 19 31.9	701	os	tran	sheet	transition	yes	/	2bi-iii
D14c	N 64 00 46.3, W019 19 31.9	701	os	pum	sheet	transition	yes	/	2bi-iii
D15a	N 64 00 47.0, W019 19 32.0	711	os	ob	sheet	transition	yes	/	2bi-iii
D15b	N 64 00 47.0, W019 19 32.0	711	os	tran	sheet	transition	yes	/	2bi-iii
D15c	N 64 00 47.0, W019 19 32.0	711	os	pum	sheet	transition	yes	/	2bi-iii
D16a	N 64 00 47.4, W019 19 33.7	722	os	ob	sheet	transition	yes	/	2bi-iii
D16b	N 64 00 47.4, W019 19 33.7	722	os	tran	sheet	transition	yes	/	2bi-iii
D16c	N 64 00 38.0, W019 19 10.7	722	os	pum	sheet	transition	yes	/	2bi-iii
D22	N 64 00 55.8, W019 19 40.1	720	pl [c]	ob	misc. [e]	? [f]	yes	yes	/

a elevations determined by handheld GPS. The uncertainty for these measurements is ±10 m b	the unit to which the sample belongs according to the geological map of Tuffen et al. (2008), where a full description and interpretation of each lithofacies can be found. See **Figure 3** for a modified version, with brief facies descriptions where cj = columnar jointed lava lobes, iv = irregular vesicular peperitic lavas, cba = crudely bedded ash, mb = massive obsidian and pumice breccia, pl = perlitised lava and os = massive breccia with obsidian sheets.

c	a non-perlitised sample from the 'perlitised lava' facies described in Tuffen et al. (2008)

d	sample description where ob = low vesicularity obsidian, pum = highly vesicular pumice, tran = transitional between dense obsidian and vesicular pumice

e	'misc.' refers to poorly exposed mound of dense obsidian

f	'?' refers to a sample from which the eruptive behaviour at that locality cannot be inferred

g	reference to sample photographs where a more detailed locality description can be found

3.2 Water concentration measurements using infra-red spectroscopy

Dissolved water contents were measured using Fourier Transform Infrared Spectroscopy (FTIR). Samples were doubly hand-polished to create wafers with thicknesses measured using a Mitutoyo digital displacement gauge accurate to ±3 µm. FTIR measurements were carried out on the same spot as measured by the displacement gauge. FTIR analysis was done at the Open University, Milton Keynes, with a Thermo Nicolet Continuum Analytical microscope, a KBr beamsplitter, a liquid nitrogen cooled MCT-A detector and a N_2 purged tank to reduce background contamination. For every sample a background (of 256 scans) was performed, followed by ≥5 analyses, with 256 scans collected between 650 and 5000 cm^{-1}, a 100 µm square aperture and 4 cm^{-1} resolution. A 15 point linear baseline correction was applied to the resulting spectra (**Fig. 4**). Peak heights were converted into water contents (C_{H2O}) using the Beer-Lambert Law:

$$C_i = \frac{M_i Abs}{d\rho\varepsilon} \quad \text{Equation 1}$$

where i refers to the volatile species of interest, M_i is molecular weight, *Abs* is absorbance (measured peak height), d is sample thickness (in cm), ρ is sample density (in g l^{-1}) and ε is the absorption coefficient (in l mol^{-1} cm^{-1}).

The 3,550 cm^{-1} and 1,630 cm^{-1} peaks were used to measure total water (H_2O_t) and molecular water (H_2O_m) (**Fig. 4**), using absorption coefficients of 80 l mol^{-1} cm^{-1} (Leschik et al.,

2004) and 55 l mol^{-1} cm^{-1} (Newman et al., 1986) respectively. Spectra were rejected in which the strong H_2O_t absorption band was saturated; for a mean sample value to be considered reliable, we required a minimum of three of the spectra to be usable. The density of Dalakvísl obsidian was taken to be 2.41 ±0.01 g cm^{-3} based on density measurements of non-vesicular samples using the Archimedes method. The molecular weight of water is 18.02 g mol^{-1}.

None of the samples produced a measureable 4,520 cm^{-1} hydroxyl (OH^-) peak, due to the combination of low wafer thickness (<200 µm) and water content of <1 wt.% (Okumura et al., 2003; Leschik et al., 2004). Similarly, the 2,350 cm^{-1} peak was always indiscernible, therefore CO_2 concentrations are deemed to fall beneath the detection limit of 30 ppm (**Fig. 4**).

As demonstrated in Owen et al. (2012), error values are highly influenced by sample thickness. For typical Dalakvísl samples, H_2O_t error is ±7.0% and comparative error is considerably smaller (±2.4%) as the same methodology and absorption coefficients were used for all samples (Owen, 2013). This is within the 10 % H_2O_t error value commonly used in FTIR studies (e.g. Dixon et al., 1995; Dixon and Clague, 2001; Dixon et al., 2002; Nichols et al., 2002; Nichols and Wysoczanski, 2007; Tuffen and Castro, 2009; Tuffen et al., 2010). Larger H_2Om error, up to ±20% (Dixon and Clague, 2001; Dixon et al., 2002), is partially due to a hidden alumina-silicate peak at 1600 cm^{-1} (Newman et al., 1986). However, in this study, H_2O_m is only used in a relative fashion, to identify hydrated samples.

3.3 Geochemistry

A small but representative sub-set of four samples was analysed for geochemistry. Bulk rock major and trace element concentrations were measured using the X-Ray

Fluorescence (XRF) facility at the University of Edinburgh with a Panalytical PW2404 wavelength-dispersive sequential X-ray spectrometer. Errors were determined by repeatedly analysing standards of known composition (Owen, 2013).

4 Results

4.1 Dissolved water content (FTIR)

Of the 29 samples analysed for water contents using FTIR, nine failed to produce any useable results due to peak saturation, reflecting difficulty in preparing sufficiently thin wafers of vesicular samples. Thus, a data-set of 20 samples was produced (**Table 2**).

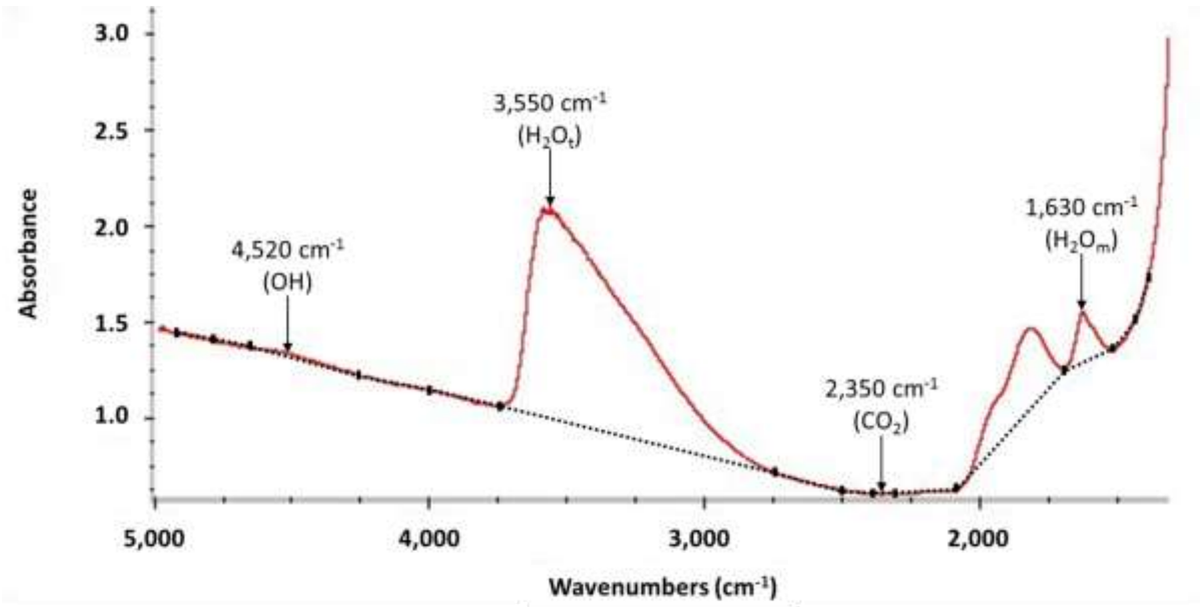

Figure 4: A typical FTIR spectrum (sample D22). The small black rectangles and dashed line mark the position of the 15 point baseline correction before it has been applied. Peaks of interest are indicated.

H_2O_t and H_2O_m peaks are seen in every spectrum but OH^- and CO_2 peaks are always too small to accurately measure.

Table 2: Averaged FTIR data. Errors for H_2O_t and H_2O_m are ± 7-10% and 20% respectively, although comparative errors will be considerably smaller. Modified from Owen et al. (2013b).

Sample name	**Sample thickness (µm)[a]**	**FTIR points per sample[b]**	**Total water (H_2O_t)**			**Molecular water (H_2O_m)**		
			3,550 peak height[c]	**Mean H_2O_t (wt.%)[d]**	**St. dev. H_2O_t (wt.%)[e]**	**1,630 peak height[c]**	**Mean H_2O_m (wt.%)[d]**	**St. dev. H_2O_m (wt.%)[e]**
D1	312	5	2.141	0.64	0.03	0.616	0.27	0.01
D3	95	5	0.594	0.58	0.02	0.153	0.22	0.03
D4	89	4	0.593	0.62	0.02	0.279	0.42	0.02
D5a	109	5	0.887	0.76	0.03	0.219	0.27	0.02
D5b	141	31	0.498	0.33	0.08	0.108	0.10	0.01
D6	47	5	0.349	0.69	0.03	0.126	0.36	0.03
D8	294	5	1.702	0.54	0.02	0.450	0.21	0.00
D9	58	5	0.530	0.85	0.01	0.142	0.33	0.02
D10	77	5	0.411	0.50	0.04	0.109	0.19	0.01
D11c	214	3	1.601	0.70	0.01	0.918	0.58	0.03
D12a	186/259	10	1.604	0.67	0.02	0.295	0.18	0.01
D12b	304	5	1.914	0.59	0.01	0.343	0.15	0.01
D13a	348	5	2.375	0.64	0.01	0.452	0.18	0.00
D13b	330	4	2.038	0.58	0.07	0.355	0.15	0.01
D14b	333	5	1.995	0.56	0.03	0.322	0.13	0.01
D14c	282	1	1.882	0.62	/	0.906	0.44	/
D15a	345	5	2.101	0.57	0.01	0.415	0.16	0.01
D16a	245	5	1.337	0.51	0.01	0.224	0.12	0.00
D16b	308	5	1.600	0.48	0.00	0.261	0.12	0.00
D22	204	5	1.170	0.53	0.04	0.286	0.19	0.05

Nine samples with saturated 3,550 cm^{-1} peaks are excluded.
CO_2 and OH^- were always below detection limit and are thus excluded.

D14c is shown in this table and also in the speciation plot (**Figure 6**) but as only one spectrum was deemed useable (and is suspected of hydration – section 4.3.1) is excluded from reconstructions of palaeo-pressure.

a Single measurement of sample thickness at location (within tens of microns) of FTIR analysis. With the exception of D12a where two locations on the wafer were measured.

b Number of successful FTIR measurements per sample.

c Mean absorbance levels from the 3,550 cm^{-1} (total water) and 1,630 cm^{-1} (molecular water) peaks.

d Mean total (H_2O_t) and molecular (H_2O_m) water contents calculated using the Beer-Lambert law, assuming a density of 2,415 kg m^{-3} and absorption coefficients of 80 l mol^{-1} cm^{-1} and 55 l mol^{-1} cm^{-1} respectively.

e Standard deviation on repeat measurements for total (H_2O_t) and molecular (H_2O_m) water contents.

Averaged data are shown in **Figure 5,** which is redrawn from Fig. 5 of Owen et al. (2013b). The water contents of the successfully measured samples (0.33-0.85 wt.%) indicate partial degassing, consistent with elevated quenching pressures in a subglacial eruption environment (Tuffen et al., 2010). Initially no systematic relationship between elevation and water content is evident. However, clear trends emerge when data are grouped by location and lithofacies type (**Fig. 5**).

Water contents from sheet zones 1 and 2 (square symbols) systematically decrease with elevation, consistent with quenching under a roughly flat-topped ice/water body, with quenching pressure decreasing with elevation. Zones 1 and 2 are well fitted by simple polynomial equations. Zone 1 samples are slightly more water-rich, although values converge at ~720 m elevation, indicating underlying complexities that shall be discussed. Lava lobe water contents (circular symbols) similarly decrease with elevation, but at any given elevation are more water-rich than the sheets (**Fig. 5**). The pumiceous juxtaposed obsidian is significantly more degassed than the other samples.

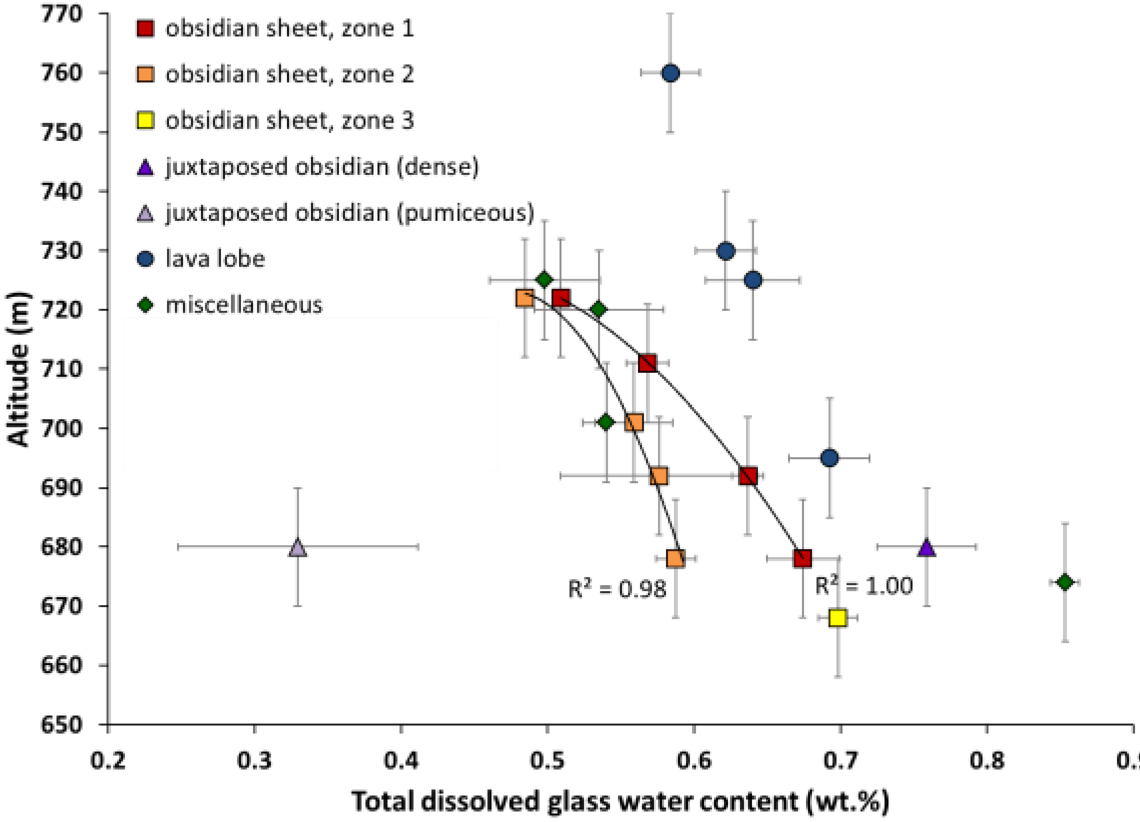

Figure 5: Water content plotted as a function of elevation, modified from Owen et al. (2013b). Symbols and colours indicate different lithofacies. Curved lines represent trendlines using a polynomial fit. Each data point represents the mean H_2O concentration from ≥3 analyses, with the standard deviation represented by the x-error bars (there is also a 10% error associated with FTIR, however comparative error is <3% for typical Dalakvísl samples). The y-error bars represent a ±10 m uncertainty in GPS measurements but comparative errors will be much smaller.

4.1.1 Water speciation

Hydrated samples must be avoided to prevent quenching pressure overestimates (Tuffen et al., 2010). Water speciation can indicate whether hydration has occurred as meteoric water is predominantly added in molecular (H_2O_m) rather than hydroxyl (OH^-) form (Yokoyama et al., 2008; Denton et al., 2009). Raw speciation data are plotted in **Figure 6**; most data fit two distinct trendlines, with trendline A encompassing all zone 1 and 2 sheet samples and with most lava lobe samples falling close to trendline B. Measurements that fit neither of these trendlines (including all pumiceous zone 3 sheet samples) have exceptionally high ratios of molecular water (labelled 'C'). These results are discussed in section 4.3.1.

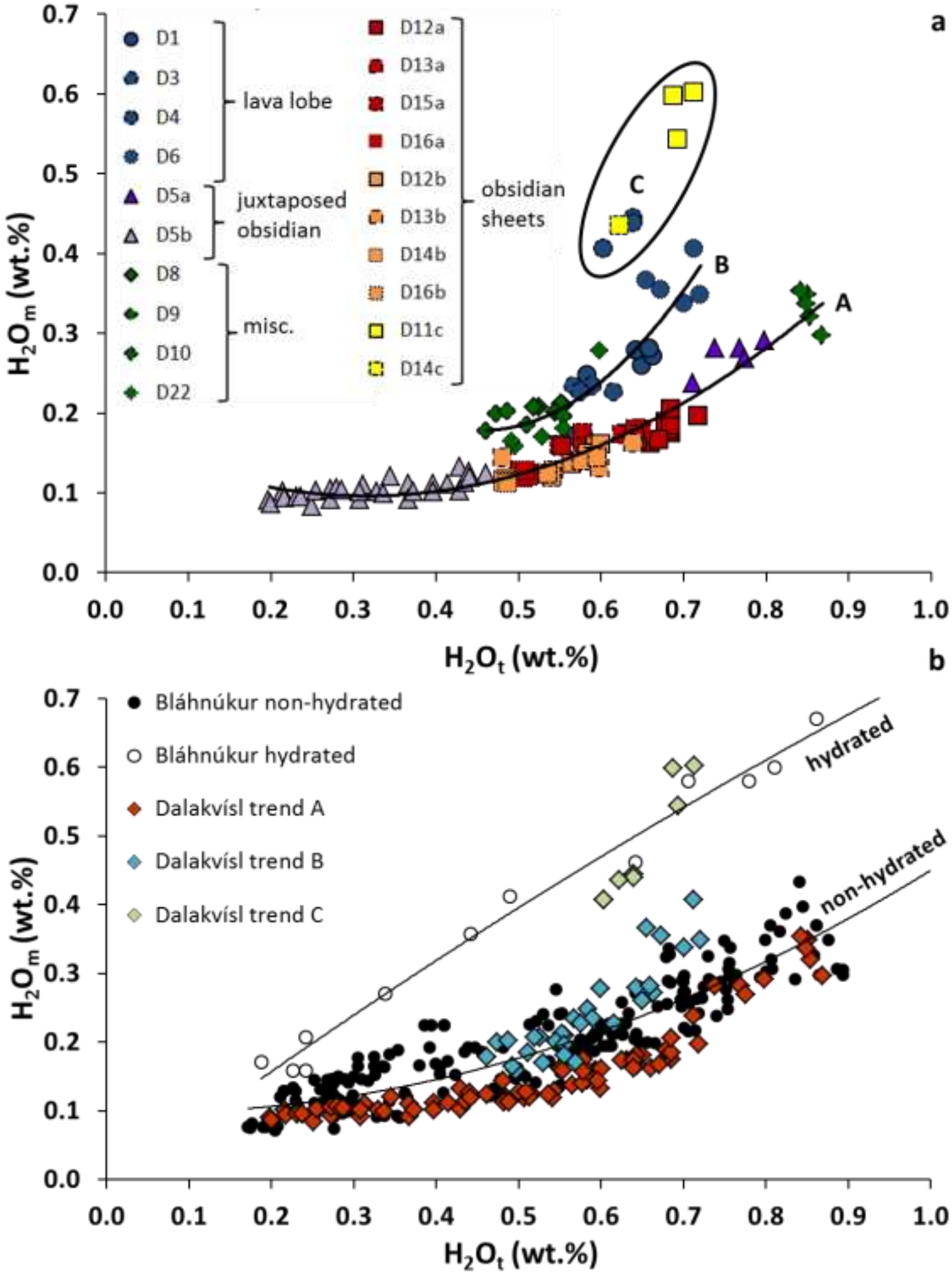

Figure 6: FTIR speciation data **(a)** Most of the raw Dalakvísl data lie close to two polynomial trendlines, labelled A and B. The circled area C indicates outliers to these trends. **(b)** Dalakvísl data superimposed on speciation data from Bláhnúkur (Owen et al., 2012) where the same absorption coefficients were

used, making direct comparisons possible. Bláhnúkur samples are readily divisible into non-hydrated and hydrated domains, as shown by the trendlines. The Dalakvísl data have been subdivided according to trends A, B and C observed in **Figure 6a**. Errors for H_2O_t and H_2O_m are 10% and 20% respectively, although comparative errors will be considerably smaller.

4.2 Geochemistry

XRF data confirms that the Dalakvísl samples are rhyolitic in composition and are compositionally similar, both in terms of major (**Table 3**) and trace element (**Fig. 7**) chemistry. Furthermore, there are strong similarities between the trace element chemistry (**Fig. 7**) of Dalakvísl and SE Rauðfossafjöll, which are both ring fracture edifices. However, there is clear distinction between Dalakvísl and Bláhnúkur, which formed in separate Torfajökull eruptions (**Fig. 1b**). Chemistry therefore concurs with the model that Dalakvísl was monogenetic (McGarvie et al., 2007) and concurrent with the SE Rauðfossafjöll eruption (McGarvie et al., 2006; Tuffen et al., 2008). The data also suggests that compositional variation was not a factor in determining the behavioural changes of the eruption.

Table 3: XRF major and trace element data for four representative samples from Dalakvísl.

	D1	**D7a**	**D13a**	**D22**	**Error**
Facies type	Lava lobe	Crudely bedded ash	Obsidian sheet	Miscellaneous	
SiO_2	72.41	70.09	71.40	71.74	0.293
TiO_2	0.42	0.39	0.39	0.39	0.030
Al_2O_3	13.30	13.12	13.09	13.32	0.270
Fe_2O_3	2.82	2.23	2.65	2.73	0.157
MnO	0.12	0.10	0.12	0.13	0.004

MgO	0.26	0.20	0.24	0.26	0.207
CaO	0.69	0.59	0.69	0.72	0.190
Na_2O	5.28	2.99	5.25	5.28	0.253
K_2O	3.91	4.27	3.86	3.87	0.043
P_2O_5	0.04	0.03	0.04	0.04	0.021
LOI	0.99	5.67	2.26	0.84	/
Total	100.24	99.66	99.99	99.32	/
AI	0.004	0.035	0.003	0.004	/
ASI	0.94	1.24	0.93	0.94	/
Classification	metaluminous	peraluminous	metaluminous	metaluminous	/
Ba	468.9	480.4	461.3	462.0	38.50
Sc	0.3	1.1	0.9	0.6	2.27
V	1.2	n.d.	n.d.	n.d.	25.23
Cr	n.d.	n.d.	n.d.	n.d.	34.23
Cu	3.0	5.4	4.1	3.3	2.83
Nb	176.7	167.7	175.6	175.5	12.37
Ni	n.d.	n.d.	n.d.	n.d.	14.97
Pb	8.6	8.6	8.2	8.4	7.35
Rb	92.3	106.4	91.7	91.9	6.13
Sr	84.5	93.8	86.4	87.4	12.13
Th	16.2	15.0	16.3	15.9	2.27
U	5.2	4.3	4.9	5.0	0.27
Y	110.9	98.4	107.7	108.0	2.63
Zn	162.2	132.6	148.3	153.8	6.43
Zr	873.0	825.5	871.3	866.5	13.60
La	117.7	113.7	116.1	116.4	4.87
Ce	243.4	234.6	241.2	239.5	11.73
Nd	108.1	102.7	106.5	106.2	5.80

Major elements are in wt.% and trace elements are in ppm

LOI Loss on ignition.

n.d. not detected.

AI alkalinity index where AI = Al-(K+Na) in molecular form; AI<0 defines peralkaline rocks whereas AI>0 defines metaluminous and peraluminous rocks (Frost and Frost, 2008).

ASI aluminum saturation index where ASI = Al/(Ca-1.67P+Na+K) in molecular form; ASI>1 defines peraluminous rocks whereas ASI<1 are metaluminous or peralkaline (Frost and Frost, 2008).

Error the maximum difference between the measured and expected values (in wt.% for major elements and ppm for trace elements) of XRF standards.

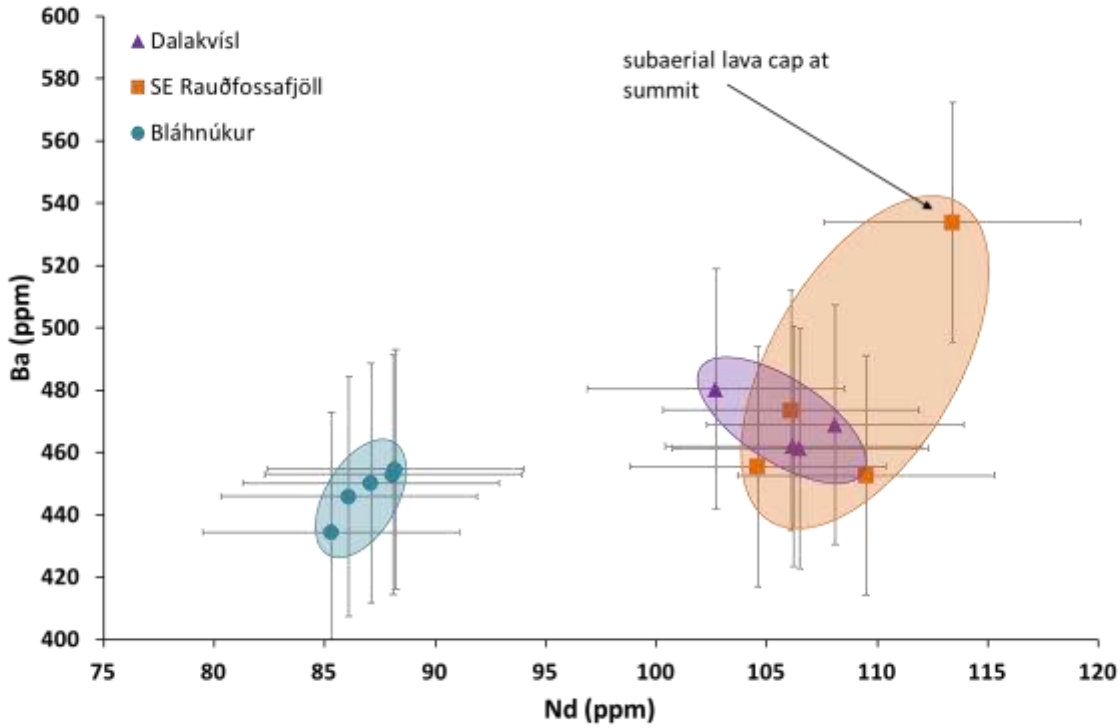

Figure 7: Trace element (XRF) data for Dalakvísl, SE Rauðfossafjöll and Bláhnúkur; three rhyolitic Torfajökull edifices, modified from Owen et al. (2012). Dalakvísl compositions (purple triangles) are closely clustered and mostly overlap with SE Rauðfossafjöll (orange squares), but plot separately from Bláhnúkur (blue circles). Error bars represent the difference between the measured and expected values of standards (**Table 3**).

4.3 Removal of data unsuitable for quenching pressure reconstruction

4.3.1 Hydrated samples

Samples plotting in field 'C' (**Fig. 6a)** have exceptionally high molecular/total water ratios, indicative of hydration, and overlap with hydrated samples from Bláhnúkur (**Fig. 6b**). Most of these samples are pumiceous and will therefore have a high surface area to volume ratio, favouring hydration. These samples are therefore excluded from the final data-set. Remaining data overlap with the non-hydrated samples from Bláhnúkur (**Fig. 6b**), thus we can be confident that these samples are non-hydrated due to their relatively low H_2O_m : H_2O_t ratios.

Distinct trendlines A and B (**Fig. 6a**) likely reflect the cooling rate dependence of water speciation (Stolper, 1982; Ihinger et al., 1999; Xu and Zhang, 2002; Di Muro et al., 2006), with slower-cooled lava lobe samples plotting at higher molecular/total water ratios (trendline B). Obsidian sheets, being smaller volume than lava lobes, cooled more rapidly and so have lower molecular/total water ratios (trendline A).

4.3.2 Post-quenching movement

Samples that have travelled downhill (either by flowing, or gravity collapse) may lead to under-estimations of palaeo-ice thicknesses, as the samples may have degassed at higher elevation and therefore lower pressure conditions prior to transportation (Moore, 1965; Macpherson, 1984; Tuffen et al., 2010).

Locality D5 consists of juxtaposed domains of obsidian with spatially variable textures, which are cut by small-scale faults (**Figs. 2ci,ii**). These textures, together with the highly degassed nature of the pumiceous sample, leads us to suspect this locality has been remobilised post-quenching, therefore these results are removed from the final data-set.

4.3.3 Equilibrium degassing

Any samples degassed under non-equilibrium conditions will not record their quenching pressures (Tuffen et al., 2010). As summarised in Rutherford (2008), many vesiculation-degassing models (e.g. Gardner et al., 1999; Mangan and Sisson, 2000) show that equilibrium degassing of rhyolite should occur at magma ascent velocities <0.7 ms^{-1}.

Estimates of magma ascent velocity at Dalakvísl are 0.001-0.01 ms^{-1}, based on inferred volume fluxes of 5-50 m^3s^{-1} (Tuffen et al., 2007) and a plausible dyke width of 5 m. The estimated velocity is similar to that estimated for explosive and effusive rhyolitic eruptions at the Inyo volcanic chain (Castro and Gardner, 2008). Independent estimates using a simple buoyant magma rise model (Höskuldsson and Sparks, 1997) and plausible dyke dimensions (1.5 km x 5 m thickness) give a lower value: 0.001 ms^{-1}. As both estimates are substantially lower than the critical ascent velocity of 0.7 ms^{-1} (Rutherford, 2008), Dalakvísl magma should meet the requirements for equilibrium water degassing.

Shallow vesiculation during explosive activity can trigger pre-quench acceleration, and thus it is conceivable that explosively generated material may have briefly exceeded the 0.7 ms^{-1} equilibration threshold at shallow conduit depths. However, disequilibrium degassing reflects the inability of magma degassing to keep track with decompression (Proussevitch and Sahagian, 1996), hence any samples degassed in disequilibrium ought to be more water-rich than their effusively erupted, equilibrium-degassed counterparts. As the opposite is true - explosively generated samples are consistently more degassed than effusively generated samples - this difference cannot reflect disequilibrium degassing.

Due to the above arguments, our samples have likely experienced equilibrium degassing and are considered suitable for palaeo-quenching pressure reconstruction. Furthermore, where samples fit well to a solubility pressure curve, degassing was arguably in equilibrium. Samples that deviate from expected water-elevation trends could have undergone disequilibrium degassing, as discussed below.

4.3.4 The final data-set of samples suitable for reconstructing palaeo-ice thickness

With the removal of hydrated (D4, D11c and D14c) and remobilised (D5a and D5b) samples, 15 samples remain suitable for palaeo-quenching pressure reconstruction (**Table 4**).

Table 1: Evidence for the Dalakvísl samples meeting the five criteria (Tuffen et al., 2010) needed to reconstruct ice thicknesses.

Criterion	Evidence to look for	Evidence at Dalakvísl	Is the criterion met?
Volatile saturation has been reached	The presence of vesicles indicates that some degassing has taken place and therefore the point of volatile saturation must have been reached [a,b] A negative relationship between elevation and water content is also evidence that degassing has taken place [c]	All but two samples (D10 & D22) have vesicles present. All samples show decreasing water contents with elevation when viewed within categories (**Fig. 5**)	Yes
Degassing was in equilibrium	Equilibrium degassing should be achieved if the ascent rate was < 0.7 ms^{-1} [d]	Eruption models suggest an eruption rate of 5-50 m^3s^{-1}, equating to a rise speed of ~10^{-2} to 10^{-3} ms^{-1} along a dyke 1.5 km long and 5 m wide [g,h]	Yes
Homogenous samples	Avoidance of complex textures and similarity between analysis of multiple data points within the same sample [a]	Most of the samples express a small standard deviation as shown by **Figure 5** and **Table 2**	Yes
No post-quenching movement	Field evidence [a]	Only two samples were collected from lava bodies that showed evidence of reworking (D5a & D5b; **Figs. 2ci,ii**) and these data have been removed	Yes

No post-quenching hydration	Perlitisation textures and high ratios of molecular water [a,e,f]	Three samples (D4, D11c & D14c) showed evidence of hydration (**Fig. 6**); these have been removed	Yes

a =(Tuffen et al., 2010); b= (Höskuldsson et al., 2006); c =(Dixon et al., 2002); d (Rutherford, 2008); e = (Yokoyama et al., 2008); f = (Denton et al., 2009); g = (Tuffen et al., 2007); h = (Höskuldsson and Sparks, 1997)

5 Discussion

5.1 Solubility pressure curves to estimate ice loading

In a monogenetic subglacial eruption, dissolved magmatic water contents typically decrease with elevation (Dixon et al., 2002; Höskuldsson et al., 2006; Schopka et al., 2006; Edwards et al., 2009) as edifice construction leads to lower pressure from overlying ice. Pressure (P in Pa) can be estimated using the formula:

$$P = \rho g h \quad \text{Equation 2}$$

where ρ is density of overlying material (in kg m^{-3}), g is gravitational acceleration (9.81 m s^{-2}), and h = thickness of overlying material (in m).

Pressures were converted into H_2O contents using the solubility model VolatileCalc (Newman and Lowenstern, 2002), assuming 0 ppm of CO_2 and a magma temperature of 800 °C, to comply with Fe-Ti oxide geothermometry estimates of 750-800 °C for Torfajökull rhyolites (Gunnarsson et al., 1998). Note that >0 ppm of CO_2 and higher magma temperatures lead to higher quenching pressures for the same dissolved water concentration (Tuffen et al., 2010).

By combining the above, we could plot expected water content as a function of elevation for various loading scenarios. Note that although, these points are an expression of water solubility as a function of depth/elevation, we chose to call the resulting curve a 'solubility pressure curve' (SPC) as ultimately the values are based on solubility-pressure relationships and this term is consistent with other studies that are pertinent to this paper (Tuffen et al., 2010; Owen et al., 2012; Owen et al., 2013b; Owen, 2016). A SPC marks the water content expected at each elevation for a given thickness of overlying ice, meltwater or rock (Schopka et al., 2006; Tuffen et al., 2010; Owen et al., 2012).

A number of different SPCs can be fitted to the Dalakvísl data, suggesting that different parts of Dalakvísl experienced different conditions that affected water solubility or magma degassing processes. Water solubility in silicic melt is principally affected by magma composition, temperature, CO_2 content and pressure (Newman and Lowenstern, 2002). Neither the measured subtle variation in sample composition (**Fig. 7**), nor plausible variations in magmatic temperature (**Fig. 8**), can sufficiently influence water solubility to explain the measured spread of water content-elevation values.

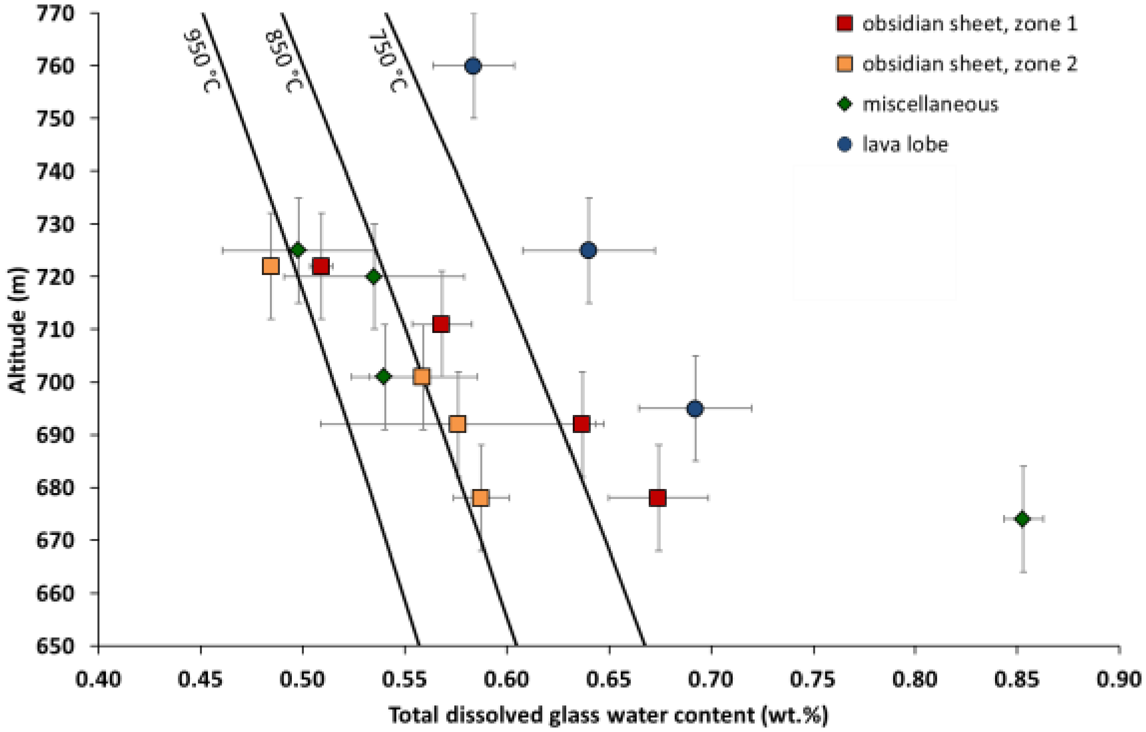

Figure 8: Measured magmatic water content-elevation relationships (symbols), with a range of modelled solubility pressure curves (SPCs), which represent different erupted temperatures (all assuming a glacier surface at 1000 m a.s.l. and loading by ice alone).

It is possible that variation in CO_2 content could affect H_2O solubility-pressure relations (Tuffen et al., 2010), but FTIR data indicate CO_2 concentrations <30 ppm. Mixed H_2O-CO_2 degassing models (Owen, 2013), based on calculations in VolatileCalc (Newman and Lowenstern, 2002), indicate maximum plausible quenched CO_2 contents of 8 ppm and 5 ppm for the least and most degassed obsidian sheets respectively and 0 ppm in the lava lobes. This assumes closed and open system degassing for the obsidian sheets and lava lobes respectively, and is based upon their pre-eruptive H_2O concentrations (Owen et al., 2013a; Owen et al., 2013b). An 8 ppm variation in CO_2 content is insufficient to explain the H_2O variation observed between the lava lobe and obsidian sheet samples (Owen et al., 2012). It is also unlikely that 8 ppm CO_2 remains as this would have required a completely closed system with a high percentage of exsolved vapour (Newman and Lowenstern, 2002) which is inconsistent with observed vesicularities (Owen et al., 2013b). Thus, we attribute distinct water solubility-elevation relationships to differences in quenching pressure, which may reflect different thicknesses/depths of overlying ice, meltwater and/or erupted deposits, or different subglacial pressure conditions.

If loading were by ice alone, a 150 m variation in ice thickness (950 to 1100 m ice surface elevation) is needed to explain the measured water content range (**Fig. 9**). The upper value of 1100 m is close to ice surface elevation estimates from subglacial-to-subaerial lithofacies transitions at nearby, contemporaneously generated ring fracture tuyas (McGarvie et al., 2006). However, models of loading by ice alone (density 917 kg m^{-3}) produce SPCs that are too steep to fit the data (**Fig. 9**), suggesting that a higher-density loading medium is required.

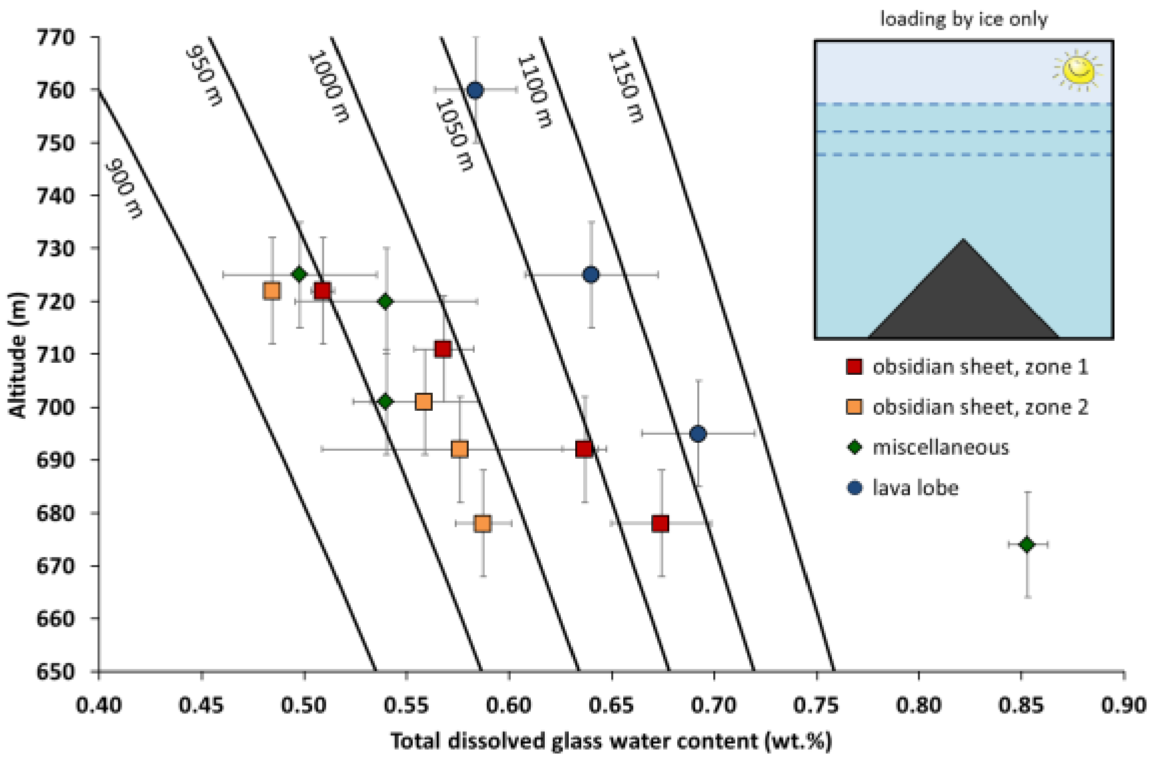

Figure 9: Measured magmatic water content-elevation relationships (symbols), with a range of modelled solubility pressure curves (SPCs), which represent different amounts of ice loading (all assuming a magma temperature of 800 °C and loading by ice alone). The inset (see legend in Figure 13) illustrates this modelled scenario for Dalakvísl (dark grey triangle), with dashed lines representing various options for ice surface elevation.

5.2 The necessity of loading from fragmental material

The strong decrease in measured water content with elevation (**Fig. 9**) requires either loading by a higher-density medium than ice or a systematic additional decrease in pressure with elevation. Indeed, field evidence suggests some Dalakvísl lithofacies formed intrusively within juvenile pyroclastic deposits, consistent with a component of loading by fragmental deposits (Tuffen et al., 2008). The density of fragmental material at Dalakvísl is estimated at 1,620 kg m^{-3}, i.e. 85% that of basaltic hyaloclastite (Höskuldsson and Sparks, 1997; Tuffen and Castro, 2009; Owen et al., 2012).

SPCs are displayed consistent with loading by fragmental deposits and with two end-member edifice morphologies – a steep-sided mound similar to the current Dalakvísl morphology (**Fig. 10**) and a flat-topped edifice similar to a tuya (**Fig. 11**). We prefer the flat-topped model (**Fig. 11**), which provides a superior data fit compared to the mound model (**Fig. 10**), and in fact allows for distinct SPCs to be matched to specific lithofacies.

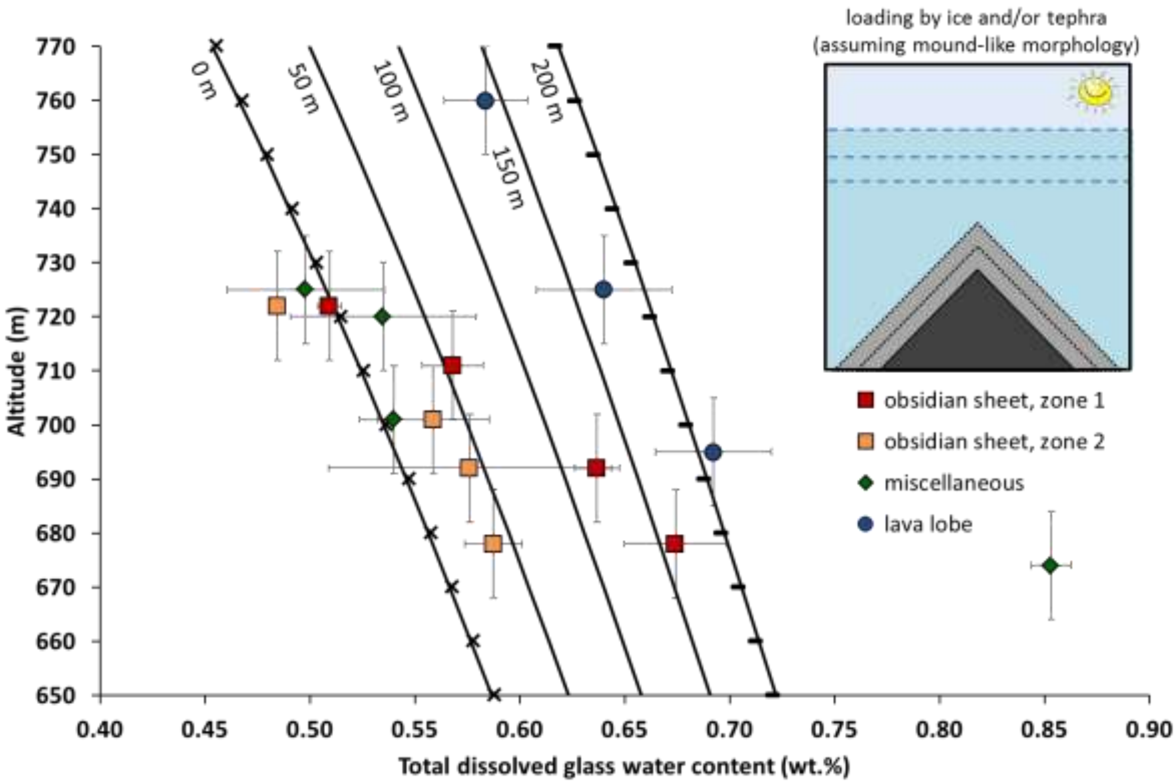

Figure 10: Measured magmatic water content-elevation relationships (symbols), with a range of modelled solubility pressure curves (SPCs), which represent different amounts of loading by ice and/or overlying fragmental material, assuming a similar mound-like morphology to Dalakvísl today. The labels at the top of each SPC indicate the thickness of fragmental material required for a 950 m ice surface. Alternatively, the SPCs could represent a change in ice elevation with constant tephra loading. For example, for loading by 100 m of fragmental material, the crossed and dashed SPCs could represent ice up to 875 m and 1,025 m a.s.l. respectively. The inset illustrates this modelled scenario for Dalakvísl (dark grey triangle), with dashed and dotted lines representing various options for ice surface elevation and original edifice size, respectively, see also legend in Figure 13.

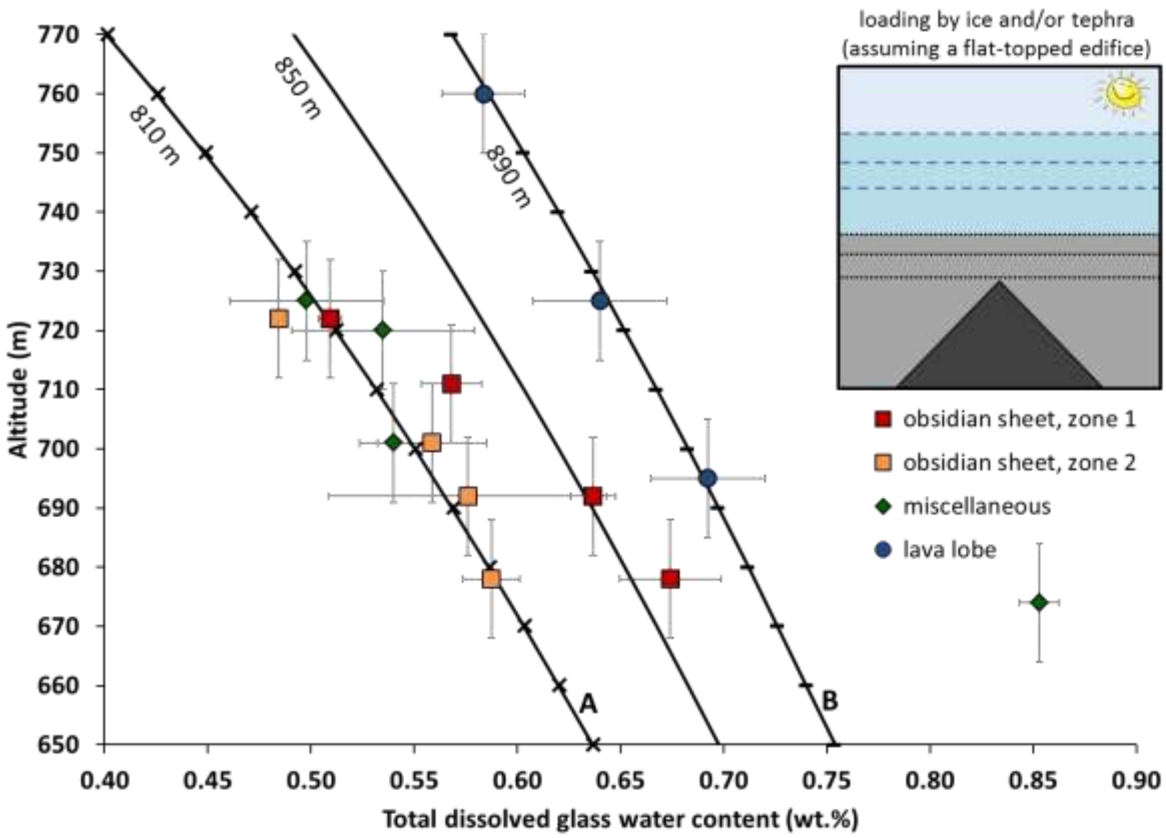

Figure 11: Measured magmatic water content-elevation relationships (symbols), with a range of modelled solubility pressure curves (SPCs), which represent different amounts of loading by ice and/or overlying fragmental material, assuming a flat-topped edifice morphology. The labels at the top of each SPC indicate various options for the surface elevations of fragmental material (i.e. edifice summit elevations) assuming that it was overlain by 70 m of ice. Alternatively, the SPCs could represent a constant edifice height with varying ice thicknesses. For example, assuming loading by fragmental material up to 850 m a.s.l., the crossed and dashed SPCs (labelled A and B respectively for reference in the text) could represent additional ice loading of 0 and 140 m respectively. The inset illustrates this modelled scenario for Dalakvísl (dark grey triangle), with dashed and dotted lines representing various options for ice surface elevation and original edifice size, respectively, see also legend in Figure 13.

In **Figure 11** the majority of the data fits to two SPCs – a high pressure SPC (B) fits the lava lobe samples and a lower pressure SPC (A) fits zone 2 sheet samples and the majority of the samples labelled ‘miscellaneous’. Zone 1 sheet samples plot between SPCs A and B but merge towards SPC A as elevation increases. Only one sample, D9 (from a poorly exposed obsidian mound), is anomalous (with ~0.85 wt.% H_2O). The excellent fit of the SPCs in **Figure 11** to the data is consistent with an originally flat-topped edifice, suggesting that all samples formed intrusively and quenched within fragmental deposits. The marked difference between the water content of sheet and lava lobe samples probably reflects spatial and/or temporal differences in overlying ice thickness, meltwater pressure and/or the height of the overlying edifice, as will be discussed.

5.3 Did Dalakvísl erupt as a tuya?

As the best-fitting SPCs require that Dalakvísl was erupted as a flat-topped edifice (**Fig. 11**), was it originally a tuya? Loading by a 27 m thick rhyolitic lava cap (density 2,415 kg m^{-3}) could replace the loading by 70 m of ice in **Figure 11.** As two distinct SPCs fit the majority of the data (**Fig. 11**), these could be explained by a double-tiered tuya (similar to SE Rauðfossafjöll, (Tuffen et al., 2002); **Fig. 12a**), with summits at 837 m and 917 m respectively. In this case, perlitised lava on the summit of Dalakvísl (Tuffen et al., 2008) could represent the now-eroded base of a lava cap; its elevation correlates well with the inferred lava cap height inferred from SPC A (**Figs. 11, 12a**). The elevation of the inferred lava cap for SPC B is higher than the preserved Dalakvísl deposits, instead matching that of the lower lava cap of SE Rauðfossafjöll (Eastern Plateau) (**Fig. 12**), thought to have erupted contemporaneously with Dalakvísl (Tuffen et al., 2008).

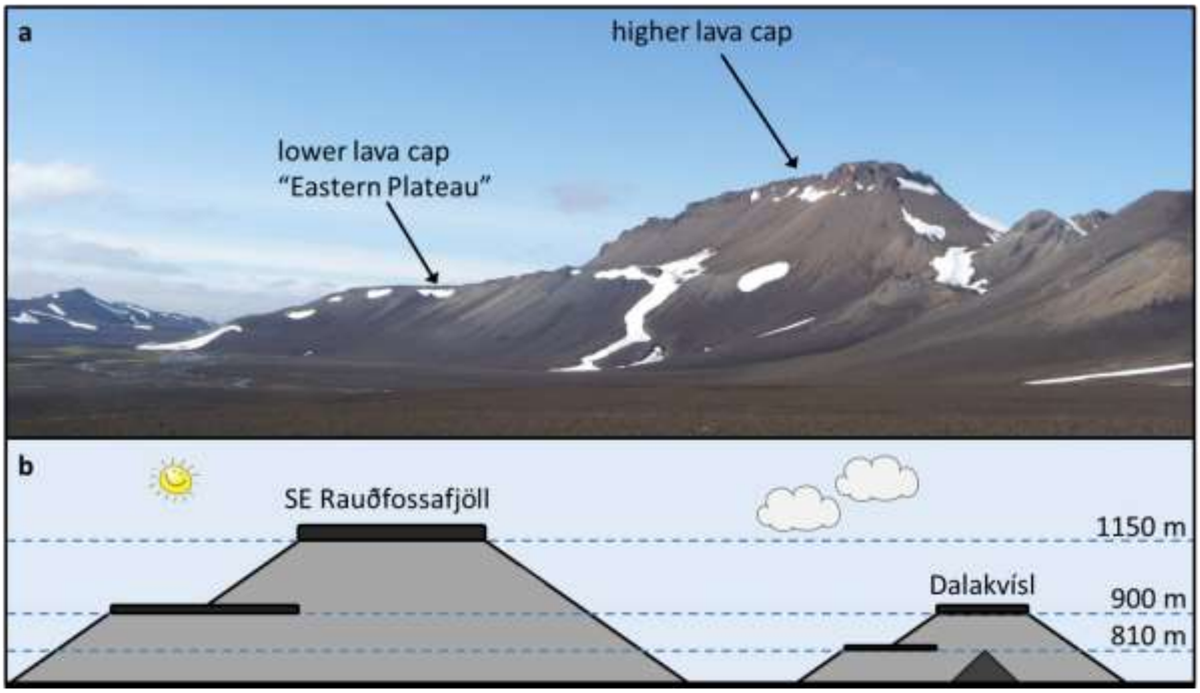

Figure 12: **(a)** SE Rauðfossafjöll, a tuya formed contemporaneously to Dalakvísl, viewed from the east. **(b)** Schematic representations of SE Rauðfossafjöll (left) and a plausible original morphology of Dalakvísl (right), with the current mophology represented by the dary grey triangle. Dark rectangles represent subaerial lava caps and pale grey represents subglacially produced deposits. The blue dashed lines show inferred paleao-ice thicknesses, see also legend in Figure 13.

The tuya model presented in **Figure 12** suggests a minimum of three ice levels during the eruption of the ring fracture rhyolites: two for Dalakvísl and two for SE Rauðfossafjöll, with the higher Dalakvísl ice surface and the lower SE Rauðfossafjöll ice surface being similar. The trace element concentrations of samples from Dalakvísl and the lower part of SE Rauðfossafjöll overlap (**Fig. 7**), with only the upper lava cap sample from SE Rauðfossafjöll having anomalous Ba contents. The Eastern Plateau and Dalakvísl may have therefore erupted together when ice surface elevation was ~900 m a.s.l., with the higher lava cap at SE

Rauðfossafjöll erupting at a different time when the ice was thicker. This is consistent with the proposal that the ring fracture rhyolites erupted during multiple but closely spaced events over an 800 year period (Brendryen et al., 2010). However, substantial erosion from Dalakvísl is required to completely remove the second lava cap at ~900 m, plus >80 m of fragmental deposits, to produce today's topography. Dalakvísl's position at a comparatively low elevation at the margin of the subglacially erupted Rauðfossafjöll massif (**Fig. 1b**) could make it particularly susceptible to erosion from eruption-triggered meltwater and during subsequent deglaciation (indeed rivers are still present today; **Figure 3**). However, it is also notable that this tuya model cannot explain the variation in vesicularity (Owen et al., 2013b) or H_2O contents (**Fig. 5**) found within the obsidian sheets. Therefore, we shall also consider alternative models.

5.4 Constraining syn-eruptive ice surface elevation

The tuya model suggests palaeo-ice thicknesses at ca. 810 m and 900 m, consistent with perlitised lava on the summit of Dalakvísl, and the elevation of the Eastern Plateau, respectively. However, we must also consider the possibility that the eruption was entirely subglacial and a lava cap never formed. SPCs A and B in **Figure 11** fit well with the water data, but we cannot directly convert loading pressures into ice thicknesses because the SPC gradients require some loading by fragmental material. Each SPC represents a range of potential ice thicknesses, coupled with various potential amounts of fragmental material. We can, however, constrain this range by assuming: (1) the edifice was flat-topped during the eruption and its surface elevation was ≥810 m (**Fig. 11**), i.e. the summit elevation today; (2) the densest loading material was fragmental deposits (1,620 kg m^{-3}); (3) the loading material with the lowest density was ice (917 kg m^{-3}); and (4) quenching pressure was equal to lithostatic/glaciostatic pressure.

For each of the two well-fitted SPCs in **Figure 11** we have thus estimated a minimum and a maximum ice surface level by applying the highest and lowest possible ratios of fragmental material to ice respectively (**Table 5**). It is highly probable that meltwater was also present as a loading material but this does not affect the minimum and maximum values as water density (1000 kg m^{-3}) falls between that of ice and hyaloclastite.

Table 2: Minimum and maximum ice surfaces estimated for solubility pressure curves A and B in **Figure 11**.

	SPC A	**SPC B**
Minimum edifice level (m a.s.l.)	810	810
Therefore maximum ice thickness (m)	70	210
Therefore maximum ice surface (m a.s.l.)	880	1,020
Minimum ice thickness (m)	0	0
Therefore maximum edifice level (m a.s.l.)	850	930
Therefore minimum ice surface (m a.s.l.)	850	930

As shown by **Table 5**, the implied ice surface level during the construction of the zone 2 sheet samples (SPC A) was 850-880 m a.s.l., whereas the lava lobes (SPC B) correspond with an ice surface of 930-1,020 m a.s.l. The maximum ice thickness was 70 and 210 m for SPCs A and B respectively. There is no overlap between the two suggested ranges in **Table 5**. One potential explanation is that a significant time gap existed between the formation of samples falling on SPCs A and B (**Fig. 11**) so that different ice surface levels could develop. However, changing subglacial pressure and under-pressured cavities are attractive alternative scenarios, as discussed below.

5.5 Two models for the order of events

Figure 11 suggests that effusive lava lobe-forming activity was associated with higher quenching pressure than more explosive obsidian sheet production. Therefore, the transition in style was either effusive to explosive, associated with a pressure reduction (**Fig. 13a**) e.g. by meltwater drainage (Owen et al., 2013b), or explosive to effusive and associated with a pressure increase (**Fig. 13b**), e.g. by increasing load of overlying tephra (Tuffen et al., 2007; Tuffen et al., 2008).

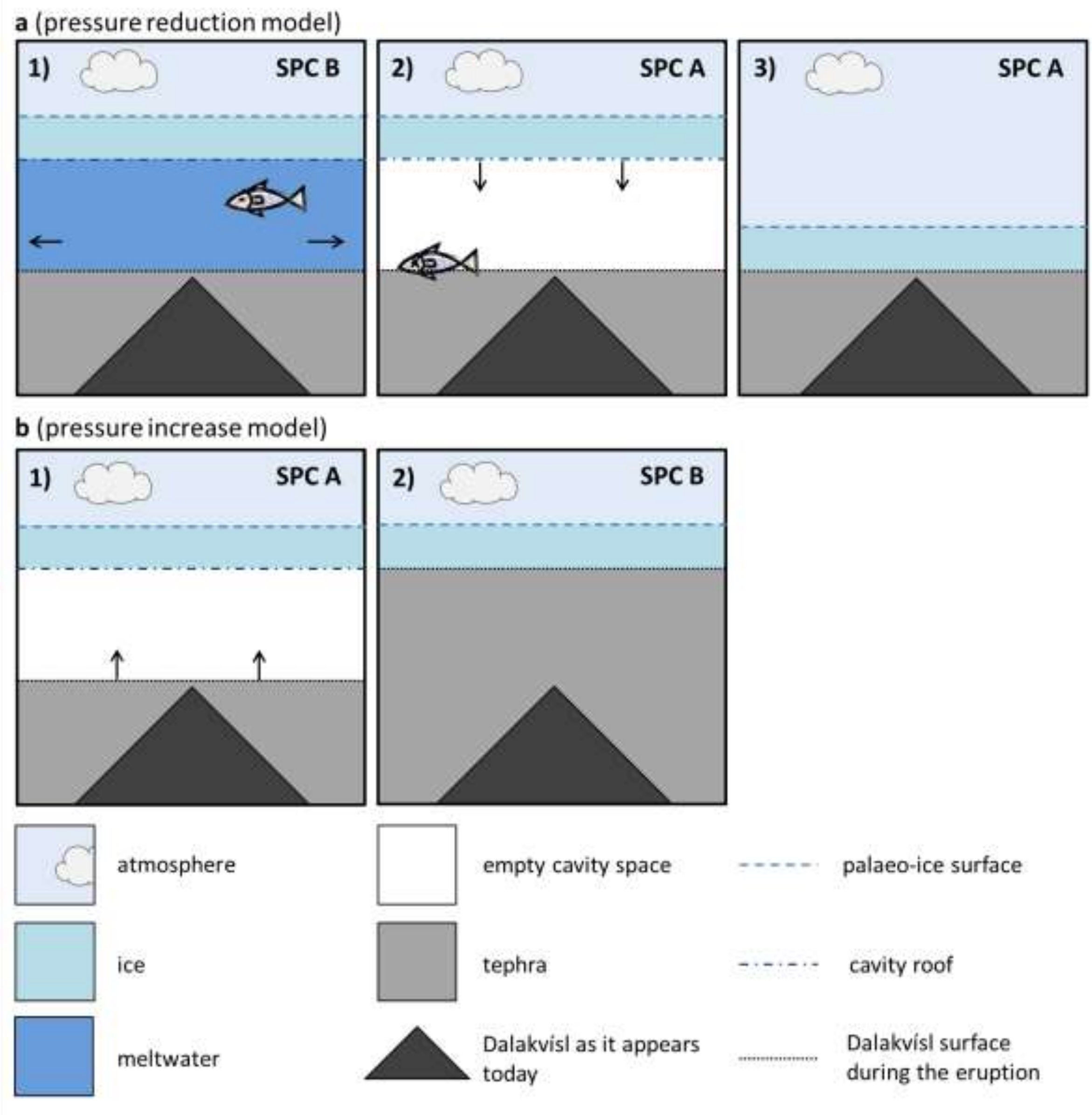

Figure 13: Schematic illustrations showing potential models for the order of events at Dalakvísl. **(a)** An initially water-filled cavity (1) drains, leading to pressure reduction; the cavity may be temporarily air-filled (2) prior to cavity closure by ice deformation (3). **(b)** An air-filled cavity (1) becomes tephra-filled, increasing confining pressure (2). Corresponding SPCs from **Figure 11** are indicated in each panel.

The pressure reduction model (**Fig. 13a**) requires the effusive lava lobes to form first (SPC B), followed by more explosive activity under a lower confining pressure regime (SPC A).

The most likely reason for a pressure reduction during a subglacial eruption is ice melting and meltwater drainage, suggesting that SPC B represents loading from a large column of ice/meltwater, whereas SPC A represents a time when the ice was much thinner and after meltwater has drained. The inferred pressure difference between SPCs A and B in **Figure 11** is 1.3 MPa. If exclusively due to meltwater drainage, this corresponds to a water level change of 130 m, which is plausible considering there was a 170-180 m drop in the Grímsvötn lake level during the 1996 Gjálp eruption (Guðmundsson et al., 2004). This pressure reduction model is still compliant with a palaeo-ice surface elevation of up to 1,020 m, as suggested in **Table 5**, which is similar to independent elevation estimates for neighbouring ring-fracture tuyas thought to have erupted contemporaneously with Dalakvísl (McGarvie et al., 2006). Furthermore, abundant <10 µm spherical bubbles within sheet cores (zone 1) are attributed to rapid decompression followed by immediate quenching (Sparks and Brazier, 1982; Larsen and Gardner, 2000; Höskuldsson et al., 2006; Stevenson, 2011; Owen et al., 2013b). The variation in H_2O content observed in the obsidian sheets (e.g. **Fig. 5**) is also consistent with rapid decompression.

The pressure increase model (**Fig. 13b**) requires initial lower-pressure explosive activity (SPC A), followed by effusive activity (SPC B) under higher confining pressure. Increased confining pressure may reflect a thickening accumulation of overlying pyroclastic debris (Tuffen et al., 2007) or blockage of meltwater drainage and subsequent pressure increase. In closed subglacial systems, the low heat content of rhyolite, in comparison to basalt, results in insufficient ice melting to accommodate the volume of the erupted deposits (Höskuldsson and Sparks, 1997). Thus, if meltwater is unable to drain, confining pressure will increase and over-pressure will develop.

Tuffen et al (2008) proposed that the obsidian sheets were emplaced as a foam, which collapsed pre-quenching due to a pressure increase, driving volatile resorption in dense sheet cores to give higher water concentrations than corresponding sheet margins. However, vesiculation-degassing modelling suggests that the difference in H_2O content between obsidian sheet zones exceeds that produced by bubble collapse and resorption alone (Owen et al., 2013b). Additionally, the rapid decrease in sheet core water contents with increasing elevation (e.g. **Fig. 11**) cannot be explained with this model. Finally, a lack of bubble collapse features and an abundance of 'decompression bubbles' within sheet cores means that vesicle textures are more consistent with rapid depressurisation rather than pressure increase (Owen et al., 2013b).

The pressure reduction model is also more consistent with independent palaeo-ice reconstructions. Problematically, both the pressure increase model and the tuya model require a significant contribution of loading from fragmental material with considerably higher density than meltwater/ice. The knock-on modelling effect is to require far lower palaeo-ice thicknesses (**Table 5**), which are inconsistent with independent estimates. Also, the strong presence of columnar-jointed obsidian, perlite, and blocky ash shards all suggest that there was abundant meltwater present during the eruption.

Considering all the arguments laid out in this section, we favour the pressure reduction model, with an initial palaeo-ice surface elevation close to 1,020 m.

Furthermore, the evidence suggests that the pressure reduction was a rapid decompression event, most likely triggered by a syn-eruption jökulhlaup. This best explains the variation in H_2O contents, vesicularities and vesicle textures of the obsidian sheets. Owen et al. (2013b) propose that a syn-eruptive jökulhlaup caused a sudden and rapid vesiculation event within the obsidian sheet deposit, which was being emplaced at the time. In the sheet margins, short diffusion distances (caused by localised shearing) permitted a rapid degassing response to the change in confining pressure, allowing existing vesicles to grow and the sheet margins to froth up. Degassing could keep pace with the pressure change, hence why these samples plot to a SPC (**Fig. 11**). However, negligible degassing took place in the dense sheet cores. Diffusion distances were too large, thus the magma responded by nucleating new bubbles, which did little to deplete the melt in volatiles. Essentially, these samples are recording non-equilibrium degassing following the pressure drop (hence not fitting to a SPC). The deviation of the zone 1 sheet samples from SPC A therefore represents the degree of disequilibrium. This decreases with elevation (**Fig. 11**), presumably as the jökulhlaup was coming to an end and degassing could more easily keep pace with changing pressure.

It is unlikely that the jökulhlaup completely drained the subglacial cavity as establishment of a hydrological connection with the glacier snout will result in degassing to atmospheric conditions (Hooke, 1984) whereas as all samples are recording elevated H_2O concentrations (e.g. **Fig. 5**).

5.6 Defining the syn-eruptive ice thickness

Assuming that SPC B represents the first phase of the eruption, an initial palaeo-ice surface between 930 and 1,020 m is required (**Table 5**). The higher end is close to inferred palaeo-ice surface elevations of 1,093 m and 1,087 m from subglacial-subaerial lithofacies transitions at the contemporaneous ring fracture edifices Illihnúkur and SW Rauðfossafjöll, respectively (McGarvie et al., 2006). As the current base of Dalakvísl is ~670 m a.s.l. (**Fig. 3**), this suggests a syn-eruptive ice thickness of ~350 m a.s.l., which is also in agreement with the ice thickness inferred by Tuffen et al. (2008).

Note that this inferred palaeo-ice thickness is based on SPC B which has been fitted to the effusive lava lobe samples. Owen et al. (2013a) and Owen et al. (2013b) speculate that effusive parts of Dalakvísl erupted under conditions of open-system degassing, which should have completely degassed in CO_2 (Owen, 2013), thus we can be confident that residual CO_2 will not be affecting the reconstructed ice thickness.

We speculate that the ice melted but drainage was hindered (Tuffen et al., 2008) until a jökulhlaup rapidly relieved pressure (Owen et al., 2013b), resulting in a new ice surface at ~880 m a.s.l. (**Table 5**). This modelling assumes 0 ppm of CO_2, but it is possible that up to 8 ppm of CO_2 remains in the obsidian sheets (Owen, 2013). However we think this unlikely due to evidence of late stage open-system degassing (Owen et al., 2013b) and the good fit of our data to the SPCs in **Figure 11**.

5.7 Defining the original edifice size and morphology

We hypothesise that the eruption constructed a near-horizontal edifice top at ~810 m a.s.l, above fragmental deposits, with an initial ice surface elevation at ~1,020 m (**Table 5, Fig. 11**). In this case, insignificant erosion has since occurred from the edifice top (current summit elevation ~810 m), but substantial erosion (up to 140 m) has occurred from the edifice margins to produce today's mound-like shape. This is consistent with the presence of perlitic lava at the Dalakvísl summit (Tuffen et al., 2008), which is more erosion-resistant than the rest of the edifice, and the presence of an actively incising stream to the south and east, where the lowest elevations occur (**Fig. 3**). If this model is correct, it means that all the samples collected formed intrusively and have since been exposed by erosion. This perhaps highlights a characteristic of subglacial rhyolitic edifices, where post quenching hydration serves to further fragment deposits (perlitisation) creating an unconsolidated pile vulnerable to erosion. By comparison, in fragmental subglacial basaltic deposits, meteoric water causes cementation and consolidation (palagonisation) of particles to form solid rock (Owen, 2016).

5.8 The relationship between explosive and effusive samples at Dalakvísl

There is a marked difference between water-rich, effusively generated and water-poor, explosively generated glasses (**Fig. 11**). Mechanisms of magma-water interaction in basaltic subglacial eruptions are sensitive to pressure, reflected by the marked transition from pillow lavas to hyaloclastites and hyalotuffs as edifices shoal towards ice surfaces. Explosive volcanism will be supressed at depth due to the inhibition of volatile exsolution caused by the ice/meltwater loading. In basaltic systems this transition typically occurs at depths of ~200 – 500 m, equivalent to ~2 -5 MPa confining pressure (Jones, 1970; Moore and Schilling, 1973; Allen, 1980; Schopka et al., 2006; Tuffen, 2007; Tuffen, 2010; Owen, 2016). Were eruption mechanisms at Dalakvísl similarly pressure-controlled? Samples collected from effusive lava lobes (SPC B) have H_2O contents consistent with quenching pressures of 2.7-3.7 MPa, whereas H_2O contents of the more explosive obsidian sheet samples (SPC A) are consistent with quenching pressures of 1.8-2.7 MPa (**Fig. 14**). This could indicate a critical pressure threshold of 2.7 MPa, which determined whether activity was explosive or effusive. However, we think this unlikely for the following reasons.

Unlike basaltic tuyas, rhyolitic edifices show little vertical variation in the nature of pyroclasts within the subglacial pile (Tuffen et al., 2002; Smellie, 2007; McGarvie, 2009; Stevenson et al., 2011; Owen, 2016), suggesting little sensitivity to confining pressure (Tuffen et al., 2007). Indeed at Dalakvísl, explosive facies would be expected to overlie effusive facies, however, their spatial distribution (**Fig. 3**) indicates, if anything, lateral rather than vertical divergence in degassing. Furthermore, the lowest elevation obsidian sheet would be expected to be a similar lithofacies type to the highest elevation lava lobe, due to their similar H_2O contents and inferred quenching pressures of 2.7 MPa (**Fig. 14**). The lithofacies are, however, very different (compare **Figures 2bi-iii** to **Figures 2ai,ii**).

.

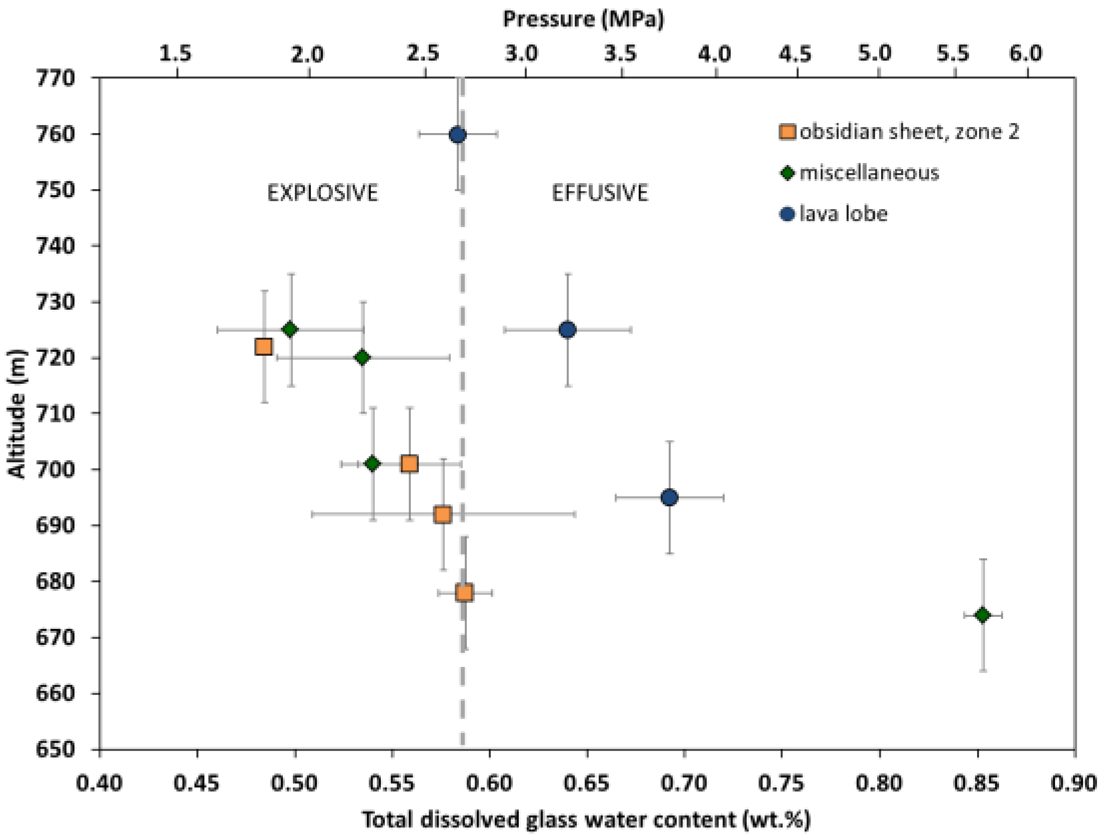

Figure 14: Measured magmatic water content-elevation relationships (symbols). Zone 1 sheet samples are not shown, due to possible non-equilibrium degassing. Pressure estimates use VolatileCalc (Newman and Lowenstern, 2002), with 0 ppm CO_2 and 800 °C magma temperature. The grey dashed line indicates the pressure that divides effusive from explosive deposits (2.7 MPa). Error bars as **Figure 5**.

Effusive and explosive deposits predominantly occur in the south and north, respectively. Therefore it is possible that both styles of activity may have occurred simultaneously, as inferred for different parts of the Gjálp 1996 fissure eruption (Guðmundsson et al., 2004). At Gjálp lateral differences in eruption style were mediated by variations in subglacial cavity pressure, controlled by local meltwater hydrology. Although this may have occurred at Dalakvísl, vesicularity and degassing of the obsidian sheets is best explained by a temporal effusive-to-explosive change.

Our preferred model is that the transition in style was triggered by a jökulhlaup. Explosive episodes have been known to follow jökulhlaup induced decompressions during subglacial basalt eruptions e.g. the 1996 Gjálp eruption (Guðmundsson et al., 2004; Höskuldsson et al., 2006) and Grímsvötn 2004 (Sigmundsson and Guðmundsson, 2004; Thordarson and Larsen, 2007; Sigmundsson et al., 2010)). It is unclear whether the decompression on its own would have been enough to cause a style transition at Dalakvísl. We suspect that the behavioural change was supplemented by a major change in the degassing behaviour of the eruption, which was albeit caused by the rapid decompression (Owen et al., 2013b).

5.9 Is there a link between ice thickness and eruptive style for Torfajökull edifices?

Interestingly, an estimate of 350 m for the Dalakvísl ice thickness is mid-way between the estimates for the palaeo-ice thickness at Bláhnúkur (400 m (Owen et al., 2012)) and SE Rauðfossafjöll (290 m (McGarvie et al., 2006; Owen et al., 2013a)). As the eruption style at Bláhnúkur was effusive (Tuffen et al., 2001; McGarvie, 2009) whereas SE Rauðfossafjöll was explosive (Tuffen et al., 2002; McGarvie, 2009) and Dalakvísl showed mixed effusive-explosive behaviour (Tuffen et al., 2008), this could be seen as showing a behavioural response to loading pressure, with edifices that formed under lower pressures being more susceptible to explosive activity. However, as the inferred ice thicknesses only vary by ~50 m this would indicate a great behavioural sensitivity towards loading pressure, which seems unlikely as all of the edifices are ≥ 140 m in height and none show a change in lithofacies with elevation within the subglacial pile. Furthermore, Angel Peak, another subglacial rhyolitic edifice within Torfajökull, erupted under an inferred ice thickness of just 120 m (Owen et al., 2013a; Owen and Tuffen, in prep.) and yet erupted effusively. This suggests that ice thickness alone cannot explain the eruptive behaviour of subglacial rhyolite. Owen et al. (2013a) concluded that there was no correlation between inferred eruptive style and palaeo-ice thicknesses for subglacial rhyolitic edifices at Torfajökull. However, the effusively produced edifices (including the effusive parts of Dalakvísl) had much lower pre-eruptive volatile contents and evidence of open system degassing, suggesting that the behaviour of subglacial rhyolite is more sensitive to degassing behaviour than ice thickness.

5.10 Conceptual model for the formation of Dalakvísl

We propose that the Dalakvísl eruption began effusively under a relatively high pressure regime, with loading by juvenile fragmental material up to a relatively flat surface at 810 m a.s.l., overlain by 210 m of ice or ponded meltwater (**Fig. 11**) i.e. with a glacier surface at ~1,020 m a.s.l. Ponding would favour sustained high meltwater pressure (Guðmundsson et al., 2004) whilst the lava lobes were being intruded into the pile of poorly consolidated juvenile hyaloclastite. Quenching pressure variations with elevation led to lava lobe samples following SPC B in **Figure 11**.

Following this, the emplacement of obsidian sheet lithofacies began as the intrusion of relatively dense bodies of obsidian within a juvenile fragmental deposit. This coincided with the onset of sudden meltwater drainage; i.e., a jökulhlaup, with a pressure decrease of 1.3 MPa, equivalent to a 130 m drop in hydrostatic head (Owen et al., 2013b). The pressure reduction allowed sheet margins to degas, but there was insufficient time to adequately degas dense sheet interiors, which instead responded by forming tiny decompression bubbles. By the time the obsidian sheets had quenched, the pressure had settled to a level ~1.3 MPa lower than previous (SPC A in **Fig. 11**). This could be represented by loading from fragmental material up to 810 m, overlain by ~70 m of ice/meltwater (**Table 5**).

Deposits erupted post-jökulhlaup were erupted in a more explosive fashion, with increased vesicularity and degree of fragmentation. Together with the pressure decrease, greater explosivity might reflect the shift to a more volatile-rich magma source and closed system degassing as supported by melt inclusion data from Owen et al. (2013a) and Owen et al. (2013b) with jökulhlaup-triggered decompression perhaps encouraging the tapping of more volatile-rich magma from depth. As explosive deposits at Dalakvísl are limited in extent and small-volume (**Fig. 3**) the explosive phase was likely a brief one.

Considerable erosion has occurred at the Dalakvísl edifice in the 70 ka since its eruption, changing the edifice shape from flat-topped to mound-like and exposing the sampled outcrops. Erosion is likely to have been driven by both glacial and fluvial processes, based on the morphology of deep stream-cut valleys on the southern and eastern basal margins (**Fig. 3**) and the local presence of younger basaltic hyaloclastite deposits, associated with reworked glacial tills, overlying the eroded upper surface of Dalakvísl formation rhyolites (Tuffen et al. 2008).

6 Conclusion

We have used the dissolved volatile content of rhyolitic glasses erupted in mixed effusive-explosive activity at Dalakvísl, Torfajökull, Iceland to infer quenching pressures and thus to place constraints on plausible syn-eruptive ice thicknesses. When grouped by lithofacies, there are decreasing trends of H_2O content with elevation, consistent with degassing in a subglacial environment. However, there is H_2O variation, both between lithofacies types and between different vesicularity zones within obsidian sheets; the dense cores (zone 1) are more water-rich than the more vesicular outer portion (zone 2) of the sheets.

Solubility pressure curves (SPCs) are used to model H_2O variations with elevation, and to reconstruct loading by ice, meltwater and volcanic deposits. Best model fits to data indicate loading by fragmental deposits and ice/water, implying that all sampled outcrops formed intrusively and have experienced significant erosion. They also suggest that the original edifice morphology was flat-topped, with a similar summit elevation to today (810 m), and therefore greatest erosion is from the edifice margins, consistent with present-day stream incision. Samples from obsidian sheet cores do not follow any SPC and are proposed to have degassed in disequilibrium, due to large diffusion distances in vesicle-poor magma and relatively rapid decompression.

Most of the data can be plotted to two SPCs, suggesting that two distinct pressure regimes operated during the eruption – a higher-pressure regime accompanied by effusive eruption style and a lower-pressure regime dominated by explosive activity. Various scenarios were modelled, including pressure changes due to variation in ice loading, tephra accumulation, subglacial cavity pressure, and water level. Our preferred model is for abrupt drainage of ponded meltwater in a jökulhlaup, to trigger rapid depressurisation to a lower pressure regime (pressure drop of 1.3 MPa, equivalent to 130 m hydrostatic head) and more explosive activity.

Best-fit models to the water-rich, early-formed lava lobes suggest up to 210 m of ice loading, with an ice surface at 930–1,020 m a.s.l., depending on the proportion of overlying fragmental material to water/ice. The upper limit fits well with independent estimates of ice surface elevation from nearby, contemporaneous tuyas, implying an initial glacier thickness of ~350 m. Interestingly, the thickness of the ice seems to have had little influence on eruptive behaviour, although it is possible that a rapid pressure change triggered the transition in style.

This paper highlights how dissolved volatile contents can provide useful insights into syn-eruptive ice thickness, edifice loading and subglacial drainage during rhyolitic eruptions under ice, provided that a large and representative sample suite is acquired, and there is a good understanding of lithofacies formation.

7 Acknowledgements

We thank the Icelandic Environment Agency, the Icelandic Centre for Research and the Icelandic Institute of Natural History for permission to conduct fieldwork and collect samples in the Fjallabak Nature Reserve. JO was funded by NERC studentship NE/G523439/1, whereas HT acknowledges NERC grants NE/G000654/1, NE/E013740/1 and a Royal Society University Research Fellowship. DMcG was supported by the Open University staff Tutor Research and Scholarship Fund. Thanks to Ferðafélag Íslands, particularly the team at Landmannalaugar (Helga, Benedikta, Rakel, Bjarney) and Fjallafang (Nína, Smári, Orri, Sarah), plus C Valentine, A Wilkinson, W Gosling, S Flude, N Odling and C Petrone for laboratory assistance, H Pinkerton, L Wilson, P Wynn, J Gilbert, M James and J Stevenson for productive discussions and J Dixon, B Edwards, S Lane and M Humphreys and others for useful edits. HT thanks the Lancaster University Facilities and Sports Centre teams for life-saving first aid and JO is grateful to the NHS and care of N Kalenderoglou. Final thanks go to J Lowenstern and M Hartley for thorough and insightful reviews which greatly improved the manuscript and especially to GB Kristjánsdóttir for an incredibly keen editorial eye.

8 References

Allen, C.C., 1980. Icelandic Subglacial Volcanism: Thermal and Physical Studies. J Geol, 88(1): 108-117. 10.1086/628478

Blake, S., 1984. Magma mixing and hybridization processes at the alkalic, silicic, Torfajökull central volcano triggered by tholeiitic Veidivötn fissuring, south Iceland. J Volcanol Geoth Res, 22(1-2): 1-31. 10.1016/0377-0273(84)90033-7

Brendryen, J., Haflidason, H. and Sejrup, H.P., 2010. Norwegian Sea tephrostratigraphy of marine isotope stages 4 and 5: Prospects and problems for tephrochronology in the North Atlantic region. Quaternary Sci Rev, 29(7–8): 847-864. 10.1016/j.quascirev.2009.12.004

Castro, J.M. and Gardner, J.E., 2008. Did magma ascent rate control the explosive-effusive transition at the Inyo volcanic chain, California? Geology, 36(4): 279-282. 10.1130/g24453a.1

Denton, J.S., Tuffen, H., Gilbert, J.S. and Odling, N., 2009. The hydration and alteration of perlite and rhyolite. J Geol Soc London, 166: 895-904. 10.1144/0016-76492008-007

Di Muro, A., Villemant, B., Montagnac, G., Scaillet, B. and Reynard, B., 2006. Quantification of water content and speciation in natural silicic glasses (phonolite, dacite, rhyolite) by confocal microRaman spectrometry. Geochim Cosmochim Ac, 70(11): 2868-2884. DOI 10.1016/j.gca.2006.02.016

Dixon, J.E., 1997. Degassing of alkalic basalts. Am Mineral, 82: 368-378. https://doi.org/10.2138/am-1997-3-415

Dixon, J.E. and Clague, D.A., 2001. Volatiles in basaltic glasses from Loihi Seamount, Hawaii: Evidence for a relatively dry plume component. J Petrol, 42(3): 627-654. https://doi.org/10.1093/petrology/42.3.627

Dixon, J.E., Filiberto, J.R., Moore, J.G. and Hickson, C.J., 2002. Volatiles in basaltic glasses from a subglacial volcano in northern British Columbia (Canada): implications for ice sheet thickness and mantle volatiles. In: J.L. Smellie and M.G. Chapman (Editors), Volcano-Ice interaction on Earth and Mars. Geological Society Special Publication No. 202, 255-271. 10.1144/gsl.sp.2002.202.01.13

Dixon, J.E. and Stolper, E.M., 1995. An Experimental Study of Water and Carbon Dioxide Solubilities in Mid-Ocean Ridge Basaltic Liquids. Part II: Applications to Degassing. J Petrol, 36(6): 1633-1646. https://doi.org/10.1093/oxfordjournals.petrology.a037268

Dixon, J.E., Stolper, E.M. and Holloway, J.R., 1995. An Experimental Study of Water and Carbon Dioxide Solubilities in Mid-Ocean Ridge Basaltic Liquids. Part I: Calibration and Solubility Models. J Petrol, 36(6): 1607-1631. https://doi.org/10.1093/oxfordjournals.petrology.a037267

Duncan, A.M., Chester, D.K. and Guest, J.E., 1986. Volcanism in Italy: The Hazard Implications of Hydromagmatic Eruptions. Interdiscipl Sci Rev, 11(4): 377-385. 10.1179/isr.1986.11.4.377

Edwards, B.R., Russell, J. and Simpson, K., 2011. Volcanology and petrology of Mathews Tuya, northern British Columbia, Canada: glaciovolcanic constraints on interpretations of the 0.730 Ma Cordilleran paleoclimate. B Volcanol, 73(5): 479-496. 10.1007/s00445-010-0418-z

Edwards, B.R., Skilling, I.P., Cameron, B., Haynes, C., Lloyd, A. and Hungerford, J.H.D., 2009. Evolution of an englacial volcanic ridge: Pillow Ridge tindar, Mount Edziza volcanic complex, NCVP, British Columbia, Canada. J Volcanol Geoth Res, 185(4): 251-275. 10.1016/j.jvolgeores.2008.11.015

Frost, B.R. and Frost, C.D., 2008. A Geochemical Classification for Feldspathic Igneous Rocks. J Petrol, 49(11): 1955-1969. 10.1093/petrology/egn054

Furnes, H., Fridleifsson, I.B. and Atkins, F.B., 1980. Subglacial volcanics - on the formation of acid hyaloclastites. J Volcanol Geoth Res, 8(1): 95-110. https://doi.org/10.1016/0377-0273(80)90009-8

Gardner, J.E., Hilton, M. and Carroll, M.R., 1999. Experimental constraints on degassing of magma: isothermal bubble growth during continuous decompression from high pressure. Earth Planet Sc Lett, 168: 201-218. https://doi.org/10.1016/S0012-821X(99)00051-5

Gonnermann, H.M. and Manga, M., 2007. The fluid mechanics inside a volcano. Annu Rev Fluid Mech, 39: 321-356. https://doi.org/10.1146/annurev.fluid.39.050905.110207

Guðmundsson, M.T., 2003. Melting of ice by magma-ice-water interactions during subglacial eruptions as an indicator of heat transfer in subaqueous eruptions. In: J.D.L. White, J.L. Smellie and D. Clague (Editors), Explosive subaqeous volcanism. American Geophysical Union Monograph, pp. 61-72.

Guðmundsson, M.T., 2005. 6. Subglacial volcanic activity in Iceland. In: C. Caseldine, A. Russell, J. Harðardóttir and Ó. Knudsen (Editors), Developments in Quaternary Sciences. Elsevier, New York, pp. 127-151. 10.1016/s1571-0866(05)80008-9

Guðmundsson, M.T., Sigmundsson, F., Björnsson, H. and Högnadóttir, T., 2004. The 1996 eruption at Gjálp, Vatnajökull ice cap, Iceland: efficiency of heat transfer, ice deformation and subglacial water pressure. B Volcanol, 66(1): 46-65. 10.1007/s00445-003-0295-9

Gunnarsson, B., Marsh, B.D. and Taylor Jr, H.P., 1998. Generation of Icelandic rhyolites: silicic lavas from the Torfajökull central volcano. J Volcanol Geoth Res, 83(1-2): 1-45. 10.1016/s0377-0273(98)00017-1

Hooke, R.L., 1984. On the role of mechanical energy in maintaining subglacial water conduits at atmospheric pressure. J Glaciol, 30(105): 180-187. 10.3189/s0022143000005918

Höskuldsson, Á. and Sparks, R.S.J., 1997. Thermodynamics and fluid dynamics of effusive subglacial eruptions. 59(3): 219-230. 10.1007/s004450050187

Höskuldsson, Á., Sparks, R.S.J. and Carroll, M.R., 2006. Constraints on the dynamics of subglacial basalt eruptions from geological and geochemical observations at Kverkfjöll, NE-Iceland. B Volcanol, 68(7-8): 689-701. 10.1007/s00445-005-0043-4

Ihinger, P.D., Zhang, Y.X. and Stolper, E.M., 1999. The speciation of dissolved water in rhyolitic melt. Geochim Cosmochim Ac, 63(21): 3567-3578. https://doi.org/10.1016/S0016-7037(99)00277-X

Imsland, P., 1983. Iceland and the ocean floor. Comparison of chemical characteristics of the magmatic rocks and some volcanic features. Contrib Mineral Petr, 83(1): 31-37. 10.1007/bf00373076

Jones, J.G., 1966. Intraglacial volcanoes of South-West Iceland and their significance in the interpretation of the form of the marine basaltic volcanoes. Nature, 212(5062): 586-588. 10.1038/212586a0

Jones, J.G., 1970. Intraglacial Volcanoes of the Laugarvatn Region, Southwest Iceland, II. J Geol, 78(2): 127-140. https://doi.org/10.1086/627496

Larsen, G., 1984. Recent volcanic history of the Veidivötn fissure swarm, southern Iceland -- an approach to volcanic risk assessment. J Volcanol Geoth Res, 22(1-2): 33-58. 10.1016/0377-0273(84)90034-9

Larsen, J.F. and Gardner, J.E., 2000. Experimental constraints on bubble interactions in rhyolite melts: implications for vesicle size distributions. Earth Planet Sc Lett, 180(1–2): 201-214. 10.1016/s0012-821x(00)00166-7

Leschik, M., Heide, G., Frischat, G.H., Behrens, H., Wiedenbeck, M., Wagner, N., Heide, K., Geißler, H. and Reinholz, U., 2004. Determination of H_2O and D_2O contents in rhyolitic glasses. Phys Chem Glasses, 45(4): 238-251.

MacDonald, R., McGarvie, D.W., Pinkerton, H., Smith, R.L. and Palavz, A., 1990. Petrogenetic evolution of the Torfajökull Volcanic Complex, Iceland I. Relationship between the magma types. J Petrol, 31(2): 429-459. 10.1093/petrology/31.2.429

Macpherson, G.J., 1984. A model for predicting the volumes of vesicles in submarine basalts. J Geol, 92(1): 73-82. www.jstor.org/stable/30062132

Mangan, M. and Sisson, T., 2000. Delayed, disequilibrium degassing in rhyolite magma: decompression experiments and implications for explosive volcanism. Earth Planet Sc Lett, 183(3-4): 441-455. http://dx.doi.org/10.1016/S0012-821X(00)00299-5

Martin, E. and Sigmarsson, O., 2007. Crustal thermal state and origin of silicic magma in Iceland: the case of Torfajökull, Ljósufjöll and Snæfellsjökull volcanoes. Contrib Mineral Petr, 153(5): 593-605. 10.1007/s00410-006-0165-5

Martin, E. and Sigmarsson, O., 2010. Thirteen million years of silicic magma production in Iceland: Links between petrogenesis and tectonic settings. Lithos, 116(1–2): 129-144. 10.1016/j.lithos.2010.01.005

Mastin, L.G., Christiansen, R.L., Thornber, C., Lowenstern, J. and Beeson, M., 2004. What makes hydromagmatic eruptions violent? Some insights from the Keanakāko'i Ash, Kīlauea Volcano, Hawai'i. J Volcanol Geoth Res, 137(1–3): 15-31. 10.1016/j.jvolgeores.2004.05.015

Mathews, W.H., 1947. Tuyas, Flat-Topped Volcanoes in Northern British-Columbia. Am J Sci, 245(9): 560-570. 10.2475/ajs.245.9.560

McGarvie, D.W., 1984. Torfajökull: A volcano dominated by magma mixing. Geology, 12(11): 685-688. 10.1130/0091-7613(1984)12<685:tavdbm>2.0.co;2

McGarvie, D.W., 2009. Rhyolitic volcano-ice interactions in Iceland. J Volcanol Geoth Res, 185(4): 367-389. 10.1016/j.jvolgeores.2008.11.019

McGarvie, D.W., Burgess, R., Tindle, A.G., Tuffen, H. and Stevenson, J.A., 2006. Pleistocene rhyolitic volcanism at Torfajökull, Iceland: eruption ages, glaciovolcanism, and geochemical evolution. Jökull, 56: 57-75.

McGarvie, D.W., MacDonald, R., Pinkerton, H. and Smith, R.L., 1990. Petrogenetic Evolution of the Torfajökull Volcanic Complex, Iceland II. The Role of Magma Mixing. J Petrol, 31(2): 461-481. 10.1093/petrology/31.2.461

McGarvie, D.W., Stevenson, J.A., Burgess, R., Tuffen, H. and Tindle, A.G., 2007. Volcano-ice interactions at Prestahnúkur, Iceland: rhyolite eruption during the last interglacial-glacial transition. Ann Glaciol, 45(1): 38-47. https://doi.org/10.3189/172756407782282453

Moore, J.G., 1965. Petrology of deep sea basalt near Hawaii. Am J Sci, 263(1): 40-52. 10.2475/ajs.263.1.40

Moore, J.G. and Schilling, J.-G., 1973. Vesicles, water, and sulfur in Reykjanes Ridge basalts. Contrib Mineral Petr, 41(2): 105-118. 10.1007/bf00375036

Newman, S., Epstein, S. and Stolper, E., 1988. Water, carbon dioxide, and hydrogen isotopes in glasses from the ca. 1340 A.D. eruption of the Mono Craters, California: Constraints on degassing phenomena and initial volatile content. J Volcanol Geoth Res, 35(1–2): 75-96. 10.1016/0377-0273(88)90007-8

Newman, S. and Lowenstern, J.B., 2002. VolatileCalc: a silicate melt–H2O–CO2 solution model written in Visual Basic for excel. Comput Geosci, 28(5): 597-604. 10.1016/s0098-3004(01)00081-4

Newman, S., Stolper, E.M. and Epstein, S., 1986. Measurement of water in rhyolitic glasses: calibration of an infrared spectroscopic technique. 71(11-12): 1527-1541.

Nichols, A.R.L., Carroll, M.R. and Höskuldsson, Á., 2002. Is the Iceland hot spot also wet? Evidence from the water contents of undegassed submarine and subglacial pillow basalts. Earth Planet Sc Lett, 202(1): 77-87. 10.1016/S0012-821X(02)00758-6.

Nichols, A.R.L. and Wysoczanski, R.J., 2007. Using micro-FTIR spectroscopy to measure volatile contents in small and unexposed inclusions hosted in olivine crystals. Chem Geol, 242(3–4): 371-384. 10.1016/j.chemgeo.2007.04.007

Okumura, S., Nakamura, M. and Nakashima, S., 2003. Determination of molar absorptivity of IR fundamental OH-stretching vibration in rhyolitic glasses. Am Mineral, 88(11-12): 1657-1662. https://doi.org/10.2138/am-2003-11-1204

Owen, J., 2013. Volatiles in Icelandic subglacial rhyolite. PhD thesis, Lancaster University.

Owen, J., 2016. Using volatiles in magma to decipher subglacial eruption dynamics. Geology Today, 32(1): 30-37. 10.1111/gto.12127

Owen, J. and Tuffen, H., in prep. On what type of volcanic edifice can you use the magma degassing technique for reconstructing palaeo-ice thicknesses?

Owen, J., Tuffen, H. and McGarvie, D.W., 2012. Using dissolved H_2O in rhyolitic glasses to estimate palaeo-ice thickness during a subglacial eruption at Bláhnúkur (Torfajökull, Iceland). B Volcanol, 74(6): 1355-1378. 10.1007/s00445-012-0601-5

Owen, J., Tuffen, H. and McGarvie, D.W., 2013a. Explosive subglacial rhyolitic eruptions in Iceland are fuelled by high magmatic H_2O and closed system degassing. Geology, 41(2): 251-254. **10.1130/G33647.1**

Owen, J., Tuffen, H. and McGarvie, D.W., 2013b. Pre-eruptive volatile content, degassing paths and depressurisation explaining the transition in style at the subglacial rhyolitic eruption of Dalakvísl, South Iceland. J Volcanol Geoth Res, 258: 143–162. https://doi.org/10.1016/j.jvolgeores.2013.03.021

Proussevitch, A.A. and Sahagian, D.L., 1996. Dynamics of coupled diffusive and decompressive bubble growth in magmatic systems. J Geophys Res, 101(B8): 17447-17455. https://doi.org/10.1029/96JB01342

Rutherford, M.J., 2008. Magma Ascent Rates. In: K.D. Putirka and F.J. Tepley III (Editors), Minerals, Inclusions and Volcanic Processes. Reviews in Mineralogy and Geochemistry, 69, 241-271. DOI 10.2138/rmg.2008.69.7

Sæmundsson, K., 1972. Jarðfræðiglefsur um Torfajökulssvæðið. Natturufræðingurinn, 42: 81–99.

Sæmundsson, K., 1979. Outline of the geology of Iceland. Jökull, 29: 7-28.

Saubin, E., Tuffen, H., Gurioli, L., Owen, J., Castro, J.M., Berlo, K., McGowan, E., Schipper, C.I. and Wehbe, K., 2016. Conduit dynamics in transitional rhyolitic activity recorded by tuffisite vein textures from the 2008-2009 Chaitén eruption. Front Earth Sci, 4. 10.3389/feart.2016.00059

Schopka, H.H., Guðmundsson, M.T. and Tuffen, H., 2006. The formation of Helgafell, southwest Iceland, a monogenetic subglacial hyaloclastite ridge: Sedimentology, hydrology and volcano-ice interaction. J Volcanol Geoth Res, 152(3-4): 359-377. 10.1016/j.jvolgeores.2005.11.010

Sigmundsson, F. and Guðmundsson, M.T., 2004. Gos í Grímsvötnum 1. – 6. nóvember 2004. Jökull, 54: 139-142.

Sigmundsson, F., Pinel, V., Lund, B., Albino, F., Pagli, C., Geirsson, H. and Sturkell, E., 2010. Climate effects on volcanism: influence on magmatic systems of loading and unloading from ice mass variations, with examples from Iceland. Philos T R Soc A, 368(1919): 2519-2534. 10.1098/rsta.2010.0042

Sigurdsson, H., 1977. Generation of Icelandic rhyolites by melting of plagiogranites in the oceanic layer. Nature, 269(5623): 25-28. 10.1038/269025a0

Smellie, J.L., 2007. Quaternary volcanism: subglacial landforms. In: S.A. Elias (Editor), Encyclopedia of Quaternary Sciences. Elsevier, Amsterdam.

Sparks, R.S.J. and Brazier, S., 1982. New Evidence for Degassing Processes during Explosive Eruptions. Nature, 295(5846): 218-220. 10.1038/295218a0

Stevenson, J.A., 2011. Grímsvötn 2 – What was in the plume?, Volcan01010.

Stevenson, J.A., Gilbert, J.S., McGarvie, D.W. and Smellie, J.L., 2011. Explosive rhyolite tuya formation: classic examples from Kerlingarfjöll, Iceland. Quaternary Sci Rev, 30(1-2): 192-209. 10.1016/j.quascirev.2010.10.011

Stevenson, J.A., Smellie, J.L., McGarvie, D.W., Gilbert, J.S. and Cameron, B.I., 2009. Subglacial intermediate volcanism at Kerlingarfjöll, Iceland: Magma-water interactions beneath thick ice. J Volcanol Geoth Res, 185(4): 337-351. 10.1016/j.jvolgeores.2008.12.016

Stolper, E., 1982. Water in silicate-glasses: An infrared spectroscopic study. Contrib Mineral Petr, 81(1): 1-17. https://doi.org/10.1007/BF00371154

Thordarson, T. and Larsen, G., 2007. Volcanism in Iceland in historical time: Volcano types, eruption styles and eruptive history. J Geodyn, 43(1): 118-152. 10.1016/j.jog.2006.09.005

Tómasson, H., 1996. The jökulhlaup from Katla in 1918. Ann Glaciol, 22: 249-254. 10.1017/S0260305500015494

Tuffen, H., 2007. Models of ice melting and edifice growth at the onset of subglacial basaltic eruptions. J Geophys Res, 112(B3). 10.1029/2006JB004523

Tuffen, H., 2010. How will melting of ice affect volcanic hazards in the twenty-first century? Philos T R Soc A, 368(1919): 2535-2558. 10.1098/rsta.2010.0063

Tuffen, H. and Castro, J.M., 2009. The emplacement of an obsidian dyke through thin ice: Hrafntinnuhryggur, Krafla Iceland. J Volcanol Geoth Res, 185(4): 352-366. 10.1016/j.jvolgeores.2008.10.021

Tuffen, H., Gilbert, J. and McGarvie, D., 2001. Products of an effusive subglacial rhyolite eruption: Bláhnúkur, Torfajökull, Iceland. B Volcanol, 63(2): 179-190. 10.1007/s004450100134

Tuffen, H., McGarvie, D.W. and Gilbert, J.S., 2007. Will subglacial rhyolite eruptions be explosive or intrusive? Some insights from analytical models. Ann Glaciol, 45(1): 87-94. 10.3189/172756407782282534

Tuffen, H., McGarvie, D.W., Gilbert, J.S. and Pinkerton, H., 2002. Physical volcanology of a subglacial-to-emergent rhyolitic tuya at Rauðufossafjöll, Torfajökull, Iceland. In: J.L. Smellie and M.G. Chapman (Editors), Volcano-Ice interaction on Earth and Mars. Geological Society Special Publication No. 202, 213-236. https://doi.org/10.1144/GSL.SP.2002.202.01.11

Tuffen, H., McGarvie, D.W., Pinkerton, H., Gilbert, J.S. and Brooker, R.A., 2008. An explosive-intrusive subglacial rhyolite eruption at Dalakvísl, Torfajökull, Iceland. B Volcanol, 70(7): 841-860. 10.1007/s00445-007-0174-x

Tuffen, H., Owen, J. and Denton, J., 2010. Magma degassing during subglacial eruptions and its use to reconstruct palaeo-ice thicknesses. Earth-Sci Rev, 99(1-2): 1-18. 10.1016/j.earscirev.2010.01.001

Xu, Z. and Zhang, Y., 2002. Quench rates in air, water, and liquid nitrogen, and inference of temperature in volcanic eruption columns. Earth Planet Sc Lett, 200(3–4): 315-330. 10.1016/s0012-821x(02)00656-8

Yokoyama, T., Okumura, S. and Nakashima, S., 2008. Hydration of rhyolitic glass during weathering as characterized by IR microspectroscopy. Geochim Cosmochim Ac, 72(1): 117-125. 10.1016/j.gca.2007.10.018

Zellmer, G.F., Rubin, K.H., Grönvold, K. and Jurado-Chichay, Z., 2008. On the recent bimodal magmatic processes and their rates in the Torfajökull–Veidivötn area, Iceland. Earth Planet Sc Lett, 269(3–4): 388-398. 10.1016/j.epsl.2008.02.026